

# ResearchOnline@JCU

This file is part of the following reference:

**Kazum, Oluwole (2014) *Electrochemical corrosion behaviour of nanostructured bainitic steel*. MPhil thesis, James Cook University.**

Access to this file is available from:

<http://researchonline.jcu.edu.au/41344/>

*The author has certified to JCU that they have made a reasonable effort to gain permission and acknowledge the owner of any third party copyright material included in this document. If you believe that this is not the case, please contact*

*[ResearchOnline@jcu.edu.au](mailto:ResearchOnline@jcu.edu.au) and quote  
<http://researchonline.jcu.edu.au/41344/>*

**ELECTROCHEMICAL CORROSION BEHAVIOUR  
OF NANOSTRUCTURED BAINITIC STEEL**

Thesis submitted  
by  
**Oluwole Kazum**

January 2014

for the degree of Masters of Philosophy  
School of Engineering and Physical Sciences  
James Cook University, Australia

## STATEMENT OF ACCESS

I, the undersigned, the author of this thesis, understand that James Cook University will make it available for use within the University Library and, by microfilm or via other means, allow access to users in other approved libraries.

I understand that generally thesis has protection under the copyright Act and wish to place no further restriction on access to this thesis.

3/01/2014

-----

Oluwole Kazum

-----

## DECLARATION

I declare that this thesis is my own work and has not been submitted in writing or electronic form for another degree or diploma at any other institution of learning. Information derived from the published or unpublished work of others has been acknowledged in the text and a list of references is given.

3/01/2014

-----  
Oluwole Kazum

## **ACKNOWLEDGEMENTS**

I express my appreciation to my academic supervisors, Dr. Bobby Mathan and Prof. Yinghe He for their support, advice and critical analysis of every stage of my work at James Cook University, Townsville.

I also want to acknowledge S. Khoddam, H. Beladi, I. B. Timokhina and P. D. Hodgson for supplying the samples and for some technical discussions.

My thanks go to my entire family for their strong support and encouragement during my postgraduate studies. I express my gratitude to my sponsor Dr. O. J. Kazum and his family for their encouragement and financial support throughout my study.

I am equally grateful for the assistance and words of encouragement from my other laboratory mates: R. Walter, A. Alabbasi and A. Baloch. Further appreciation goes to the entire academic and administrative staff of the School of Engineering and Physical Sciences, James Cook University, Townsville.

## ABSTRACT

Nanostructured bainitic steels are gaining high interest due to their excellent mechanical properties. However, high carbon content in nanostructured bainitic steels can influence their general and localized corrosion susceptibility. In this study, the corrosion behaviour of nanostructured bainitic steel was compared with the well-known martensitic steel in chloride-containing solution using electrochemical techniques such as electrochemical impedance spectroscopy (EIS) and potentiodynamic polarisation. EIS results showed that the polarisation resistance ( $R_p$ ) for nanostructured bainitic steel ( $3400 \Omega \text{ cm}^2$ ) was higher than that of martensitic steel ( $2000 \Omega \text{ cm}^2$ ). Potentiodynamic polarisation results showed an 85% lower corrosion current density ( $i_{corr}$ ) for nanostructured bainitic steel as compared to martensitic steel. Interestingly, galvanostatic polarisation of the steels showed different corrosion morphology, i.e., martensitic steel revealed intergranular corrosion (IGC) and the nanostructured bainitic steel exhibited lamellar structure suggesting selective dissolution.

In order to understand the corrosion mechanism of the nanostructured bainitic steel, two different isothermal temperatures were used to produce nanostructured bainitic steel with different percentages of retained austenite (RA) and bainitic ferrite (BF). Nanostructured bainite formed at 200 °C (RA: 21%) exhibited marginally higher corrosion resistance compared with that at 350 °C (RA: 53%). Post-corrosion analysis of the galvanostatically polarised samples revealed localised corrosion for both the steels, but the degree of attack was higher in the 350 °C steel than in the 200 °C steel. The localised corrosion attack was due to the

selective dissolution of the RA phase. The higher volume fraction and larger size of RA in the 350 °C steel as compared to that of the 200 °C steel contributed to the pronounced corrosion attack in the 350 °C steel.

To enhance the corrosion resistance of the nanostructured bainitic steel, a conducting polymer, polyaniline (PANI), was coated on the steel using galvanostatic method. Samples coated for 10 mins with lower current density (5 mA cm<sup>-2</sup>) exhibited higher  $R_p$  ( $3.2 \times 10^4 \Omega \text{ cm}^2$ ) as compared to the samples coated with 20 mA cm<sup>-2</sup> ( $9.82 \times 10^3 \Omega \text{ cm}^2$ ). Although the  $R_p$  of the coating increased with increase in the coating thickness (i.e., by increasing the coating time), under long-term exposure the  $R_p$  of the coated samples dropped drastically. This can be attributed to the large pores in the coatings. To reduce the porosity in the coating, the coating process was performed under stirred-condition. The stirred-condition coating (20 mA cm<sup>-2</sup> for 20 mins) exhibited only a few fine defects and the  $R_p$  was almost two orders of magnitude higher than that of the unstirred-condition coated sample. Long-term EIS results for the stirred-condition coated sample showed an initial increase in  $R_p$  ( $4.3 \times 10^6 \Omega \text{ cm}^2$ ) after 78 h exposure, and then gradually decreased to  $7.0 \times 10^5 \Omega \text{ cm}^2$  after 168 h exposure. However, the  $R_p$  was significantly higher than that of the bare metal. Potentiodynamic polarisation results confirmed the higher corrosion resistance of the stirred-condition coated sample as compared to the unstirred-condition coated sample.

The study suggests that nanostructured bainitic steel exhibited higher corrosion resistance than martensitic steel in chloride-containing solution, but the RA in the nanostructured bainitic steel dissolved selectively. PANI coating using

galvanostatic method under stirred-condition, however, improved the general and localized corrosion resistance of nanostructured bainitic steel significantly.

The findings from this dissertation have been disseminated through the following publications.

**Journal Papers:**

- O. Kazum, M. Bobby Kannan, H. Beladi, I.B. Timokhina, P.D. Hodgson, S. Khoddam, “Aqueous corrosion performance of nanostructured bainitic steel” *Material & Design* 54 (2014) 67-71.
- O. Kazum, M. Bobby Kannan, H. Beladi, I.B. Timokhina, P.D. Hodgson, S. Khoddam, “Selective dissolution of retained austenite in nano-bainitic steel” *Advanced Engineering Materials* 15 (2013) 1-3.
- O. Kazum, M. Bobby Kannan, “Galvanostatic polymerization of aniline on steel: improving the coating performance in chloride-containing environment” *Synthetic Metals* 180 (2013) 54-58.

**Conference Paper:**

- O. Kazum, M. Bobby Kannan, “Galvanostatic coating of polyaniline on steel” *ACA Corrosion and Prevention*, Brisbane, Nov 14-19, 2013.

## TABLE OF CONTENTS

|  |      |
|--|------|
| Statement of Access.....                   | ii   |
| Declaration.....                           | iii  |
| Acknowledgements.....                      | iv   |
| Abstract.....                              | v    |
| Table of Contents.....                     | viii |
| List of Figures.....                       | xi   |
| List of Tables.....                        | xiii |
| List of Symbols.....                       | xiv  |
| <br>                                       |      |
| Chapter 1: Introduction.....               | 1    |
| 1.1 Background.....                        | 1    |
| 1.2 Objectives.....                        | 2    |
| <br>                                       |      |
| Chapter 2: Literature Review.....          | 3    |
| 2.1 Steel.....                             | 3    |
| 2.2 Bainite in Steel.....                  | 3    |
| 2.3 Corrosion of Steel.....                | 5    |
| 2.4 Types of Corrosion.....                | 6    |
| 2.4.1 Uniform Corrosion.....               | 7    |
| 2.4.2 Localized Corrosion.....             | 7    |
| 2.4.2.1 Pitting Corrosion.....             | 7    |
| 2.4.2.2 Galvanic Corrosion.....            | 8    |
| 2.4.2.3 Crevice Corrosion.....             | 9    |
| 2.4.2.4 Intergranular Corrosion.....       | 9    |
| 2.4.3 Stress Corrosion Cracking (SCC)..... | 9    |

|  |    |
|--|----|
| 2.5 Corrosion Test Methods .....                                     | 10 |
| 2.5.1 Electrochemical Impedance Spectroscopy (EIS) .....             | 10 |
| 2.5.2 Potentiodynamic Polarisation Method .....                      | 12 |
| 2.6 Corrosion Mechanisms: Effect of Microstructure .....             | 14 |
| 2.7 Corrosion Protection: Conducting Polymers .....                  | 16 |
| <br>   |    |
| Chapter 3: Materials and Experimental Procedure .....                | 22 |
| 3.1 Material Characterization .....                                  | 22 |
| 3.1.1 Material and Heat Treatment .....                              | 22 |
| 3.1.2 Microstructure Analysis .....                                  | 23 |
| 3.1.3 Test Samples Preparation .....                                 | 23 |
| <br>   |    |
| 3.2 Electrochemical Corrosion Testing .....                          | 24 |
| 3.3 Electrochemical Coating .....                                    | 25 |
| 3.3.1 Galvanostatic Technique .....                                  | 25 |
| 3.3.2 Coating Characterization .....                                 | 26 |
| <br>   |    |
| Chapter 4: Corrosion Behavior of Nanostructured Bainitic Steel ..... | 27 |
| 4.1 Aqueous Corrosion Behavior .....                                 | 27 |
| 4.1.1 Microstructure .....   | 27 |
| 4.1.2 Open Circuit Potential .....                                   | 28 |
| 4.1.3 Electrochemical Impedance Spectroscopy (EIS) .....             | 29 |
| 4.1.4 Potentiodynamic Polarisation .....                             | 30 |
| 4.1.5 Post-Corrosion Analysis .....                                  | 32 |
| 4.2 Selective Dissolution of Retained Austenite .....                | 35 |
| 4.2.1 Microstructure .....   | 35 |
| 4.2.2 Potentiodynamic Polarisation .....                             | 36 |

|  |    |
|--|----|
| 4.2.3 Post-Corrosion Analysis.....   | 38 |
| 4.2.4 Discussion .....   | 39 |
| 4.3 Summary .....  | 40 |
| <br>   |    |
| Chapter 5: Electrochemical Coating of Polyaniline on Nanostructured Bainitic Steel ..... | 41 |
| 5.1 Galvanostatic Coating .....  | 41 |
| 5.2 Electrochemical Impedance Spectroscopy (EIS) .....                                   | 42 |
| 5.3 Potentiodynamic Polarisation.....  | 44 |
| 5.4 Coating Characterization .....   | 45 |
| 5.5 Effect of Coating Time.....  | 47 |
| 5.6 Effect of Stirring on Galvanostatic Coating.....                                     | 49 |
| 5.6.1 Coating Potential .....  | 49 |
| 5.6.2 Coating Morphology .....   | 50 |
| 5.6.3 Fourier Transform Infrared Spectroscopy (FTIR) .....                               | 52 |
| 5.6.4 Electrochemical Impedance Spectroscopy (EIS) .....                                 | 53 |
| 5.6.5 Potentiodynamic Polarisation.....  | 57 |
| 5.7 Summary .....  | 58 |
| <br>   |    |
| Chapter 6: Conclusions.....  | 59 |
| 6.1 General Conclusion.....  | 59 |
| 6.2 Future Work .....  | 60 |
| <br>   |    |
| References .....   | 61 |

## LIST OF FIGURES

| Figure | Description   | Page |
|--------|---|------|
| 2.1    | Schematic of time temperature transformation (TTT) for steel  | 4    |
| 2.2    | A typical Nyquist plot  | 12   |
| 2.3    | A typical potentiodynamic polarisation scan   | 13   |
| 2.4    | Schematic of iron-iron carbide phase diagram  | 15   |
| 3.1    | Heat treatment procedure used to produce nanostructured bainitic steel  | 22   |
| 3.2    | Schematic of the three-electrode cell used for electrochemical experiments  | 24   |
| 4.1    | TEM micrographs of nanostructured bainitic steel: (a) low magnification and (b) high magnification  | 27   |
| 4.2    | Open circuit potential (OCP) curves for nanostructured bainitic steel and martensitic steel in 3.5 wt.% NaCl solution   | 28   |
| 4.3    | Nyquist plots of nanostructured bainitic steel and martensitic steel exposed to 3.5 wt.% NaCl solution  | 29   |
| 4.4    | Potentiodynamic polarisation plots for the nanostructured bainitic steel and martensitic steel in 3.5 wt. % NaCl solution                                     | 31   |
| 4.5    | SEM micrographs of galvanostatically polarised samples in 3.5 wt. % NaCl: (a and b) nanostructured bainitic steel (c and d) martensitic steel                 | 32   |
| 4.6    | SEM micrographs of samples immersed in 3.5 wt.% NaCl solution for 7 days: (a) nanostructured bainitic steel, and (b) martensitic steel                        | 33   |
| 4.7    | A schematic representation of the microstructures of nanostructured bainitic steel and martensitic steel before and after corrosion in 3.5 wt.% NaCl solution | 34   |

|      |   |    |
|------|---|----|
| 4.8  | TEM micrographs of the nanostructured bainitic steels formed at: (a and b) 200 °C (c and d) 350 °C  | 36 |
| 4.9  | Potentiodynamic polarisation curves for nanostructured bainitic steels  | 37 |
| 4.10 | SEM micrographs for galvanostatically polarised nanostructured bainitic steels formed at: (a and b) 200 °C and (c and d) 350 °C               | 38 |
| 5.1  | Potential vs. time curves for galvanostatic synthesis of aniline coating on steel   | 42 |
| 5.2  | Nyquist plot for bare and coated samples  | 43 |
| 5.3  | Potentiodynamic polarisation plot for bare metal and coated samples   | 44 |
| 5.4  | SEM micrographs for galvanostatic coatings (a and b) 5 mA cm <sup>-2</sup> (b and c) 20 mA cm <sup>-2</sup>                                   | 46 |
| 5.5  | Nyquist plot for the 5 mA cm <sup>-2</sup> coated sample obtained at various coating time   | 48 |
| 5.6  | Bar charts of $R_p$ values for 5 mA cm <sup>-2</sup> coated sample obtained at different coating time   | 48 |
| 5.7  | Potentiodynamic polarisation plot for coated sample done with 5 mA cm <sup>-2</sup>   | 49 |
| 5.8  | Galvanostatic curves of polyaniline coatings on steel under two different electrolyte bath conditions   | 50 |
| 5.9  | SEM micrographs of polyaniline coatings on steel under two electrolyte bath conditions  | 51 |
| 5.10 | FTIR spectra of polyaniline coating on steel produced using galvanostatic method under two electrolyte bath conditions                        | 52 |
| 5.11 | Nyquist plots of bare metal and polyaniline coated samples tested in 3.5 wt. % NaCl solution  | 54 |
| 5.12 | Long-term polarisation plot of polyaniline coating on steel in 3.5 wt. % NaCl solution for electrolyte in (a) unstirred (b) stirred condition | 56 |
| 5.13 | Potentiodynamic polarisation plots for the bare sample and the polyaniline coated sample electrolyte in 3.5 wt. % NaCl solution               | 57 |

## LIST OF TABLES

| Table | Description   | Page |
|-------|---|------|
| 2.1   | Mechanical properties of common steels  | 5    |
| 2.2   | Standard electromotive force (emf) series of metals   | 8    |
| 2.3   | Summary of literature on corrosion of steels  | 19   |
| 2.4   | Summary of literature on corrosion prevention by using conducting polymers  | 20   |
| 3.1   | Chemical composition of the steel used in this study  | 22   |
| 4.1   | EIS data obtained from equivalent circuit modelling of the impedance spectra  | 30   |
| 4.2   | Potentiodynamic polarisation data of the nanostructured bainitic steel and the martensitic steel in 3.5 wt. % NaCl solution | 31   |
| 5.1   | EIS data of bare metal and coated samples   | 43   |
| 5.2   | Potentiodynamic polarisation data for bare metal and coated samples   | 45   |
| 5.3   | Coating thickness data for polyaniline (PANI) coated steels   | 46   |
| 5.4   | EIS values obtained from the fit to the equivalent circuit for the impedance spectra in 3.5 wt. % NaCl solution             | 55   |
| 5.5   | Electrochemical corrosion data for the bare sample and polyaniline coated sample in 3.5 wt. % NaCl solution                 | 58   |

## LIST OF SYMBOLS

|                    |   |   |
|--------------------|---|---|
| $^{\circ}\text{C}$ | = | Degree Celsius                            |
| <i>wt.%</i>        | = | Weight in percentage                      |
| <i>TTT</i>         | = | Time temperature transformation           |
| <i>SCC</i>         | = | Stress corrosion cracking                 |
| <i>EIS</i>         | = | Electrochemical impedance spectroscopy    |
| $Z_0, Z_t$         | = | Impedance of the signal at given time     |
| $E_0, E_t$         | = | Potential of the signal at given time     |
| $I_0, I_t$         | = | Current at given time                     |
| $\varphi$          | = | Phase shift between current and potential |
| <i>CR</i>          | = | Corrosion rate                            |
| <i>F</i>           | = | Faraday constant (96485 coulomb/mole)     |
| $\rho$             | = | Density of the metal in $\text{g/cm}^3$   |
| <i>PANI</i>        | = | Polyaniline                               |
| <i>PPy</i>         | = | Polypyrrole                               |
| <i>TEM</i>         | = | Transmission electron microscope          |
| <i>SiC</i>         | = | Silicon-carbide                           |
| <i>SEM</i>         | = | Scanning electron microscope              |
| <i>rpm</i>         | = | Revolution per minute                     |
| <i>FTIR</i>        | = | Fourier transform infrared spectroscopy   |
| <i>RA</i>          | = | Retained austenite                        |
| <i>BF</i>          | = | Bainitic ferrite                          |

|                             |   |  |
|-----------------------------|---|--|
| $OCP$                       | = | Open circuit potential   |
| $R_s, R_f, R_{ct}$<br>$R_p$ | = | Resistance due to solution, film, charge transfer and polarization |
| $C_f, C_{dl}$               | = | film capacitance, double layer capacitance                         |
| $E_{corr}$                  | = | Corrosion potential  |
| $i_{corr}$                  | = | Corrosion current density  |
| $IGC$                       | = | Intergranular corrosion  |
| $SD$                        | = | Selective dissolution  |
| $GB$                        | = | Grain-boundary   |
| $min$                       | = | Minute   |
| $h$                         | = | Hour   |

## CHAPTER 1: INTRODUCTION

### 1.1 Background

The pursuit for high safety standards and weight reduction in automobiles has led to the research and development of high strength and high toughness steels. Generally high carbon steel can be transformed to high strength steel by controlled temperature transformation to form different grain microstructure. Martensitic microstructure has fairly high tensile strength and can be formed by quenching steel; however, grain refinement has become one of the most desirable methods of strengthening metallic materials because of improved properties (Ehinger et al. 2013; Xue et al. 2006; Chen et al. 2005; Martins et al. 2013).

Recently, a relatively low temperature transformation of steel has uncovered nanostructures in steel and it is popularly known as nano-bainitic steel (Beladi et al. 2009). Generally, the nanostructured bainitic steel is formed at a relatively low temperature of 150-350 ° C (Beladi et al. 2009; Roberge 2008; Timokhina et al. 2011). The steel comprises of very fine layers of bainitic ferrite laths and retained austenite films and offers a uniquely high combination of strength (~2.3 GPa), toughness (~30 MPa m<sup>1/2</sup>) and ductility (~30 %) (Garcia-Mateo et al. 2003; Caballero and Bhadeshia 2004; Caballero et al. 2007). Studies have shown that the high carbon level (0.8 wt.%) (Furuhara et al. 2006) along with low isothermal transformation process is responsible for the refinement of the bainitic ferrite laths, ranging from 20 to 300 nm in thickness depending on isothermal holding temperature (Peet et al. 2004; Avishan et al. 2013; Caballero et al. 2004; Bhadeshia 2005). The attractive mechanical properties of nanostructured bainitic steels make them a potential candidate for impact/wear resistance applications in

automobile components such as chassis, engine compartments, bumpers and side doors, as well as a range of applications in construction, offshore and defence industries. Furthermore, these steels can contribute to a significant weight and cost savings in those applications.

Corrosion is however, a major problem in steels. Extensive work has been done on corrosion of steels in chloride-containing solution. Report suggests that steels undergo uniform and localised forms of corrosion such as pitting, crevice and intergranular corrosion. For low carbon bainitic steel, the focus has been still on making the production less expensive as they require different alloying (Ti and Ni) addition and strengthening methods (Wang et al. 2011). The high carbon nanostructured bainitic steel has a great potential for engineering applications. However, its high carbon (0.8 wt.%) content is of concern, as it can influence the corrosion behaviour of the material. Hence, it is critical to understand the corrosion behaviour of this nanostructured bainitic steel. In this study the nanostructured bainitic steel was therefore compared to martensitic steel of the same composition formed using a different heat treatment.

## **1.2 Objectives**

The two main research objectives of this study were to:

- Evaluate the corrosion behaviour of nanostructured bainitic steel using electrochemical techniques.
- Enhance the corrosion resistance of nanostructured bainitic steel using conducting polymer coating.

## **CHAPTER 2: LITERATURE REVIEW**

### **2.1 Steel**

Steels are the backbone of engineering structure which offers excellent mechanical properties. In order to improve the strength of steels for load-bearing applications, carbon is commonly added as a hardener. This has its limitation as the ductility of the end product is reduced. However, the application of controlled heat treatment process has shown an enhancement of strength and retention of some percentage of the ductility paving way for a new class of material known as nanostructured bainitic steel.

### **2.2 Bainite in Steel**

Bainite consist of aggregates of plates (sheaves) of ferrite separated by untransformed austenite, cementite or martensite. When steel contains some carbide-inhibitor elements, such as silicon and aluminium the bainite can be composed of bainitic ferrite and retained austenite. Bainite are formed at cooling rates that is slower compared to that for martensitic steel but faster to that for ferrite/pearlite formation. To obtain bainitic transformation the cooling rate must be kept below the nose of the C-curve in the time temperature transformation (TTT) diagram as shown in Figure 2.1 (Charlie 1996). Generally the transformation of steel can be described by shear and diffusional mechanism (Yang et al. 2005). The bainite in steel has two forms and they are the upper and lower bainite (Sajjadi and Zebarjad 2007). The upper bainite forms at temperatures between 550 and 400 °C. Based on the carbon content and transformation temperature of the steel, different morphological structures may be formed. For low carbon steels, fine bainitic laths nucleate at the grain-boundaries

and due to its low carbon solubility, carbon is rejected into the austenite surrounding the bainitic ferrite laths. As carbon concentration increases in the austenite, cementite nucleate as discrete particles at the ferrite/austenite interfaces. The structure may appear more pearlite as in feathery bainite. The lower bainite on the other hand forms at temperatures between 400 and 250 °C. The changeover temperature between the upper and lower bainite is unknown and may depend on the carbon content of the steel. At lower temperature, rejection of carbon by diffusion does not occur so readily, so iron carbides are formed closely with bainitic ferrite.

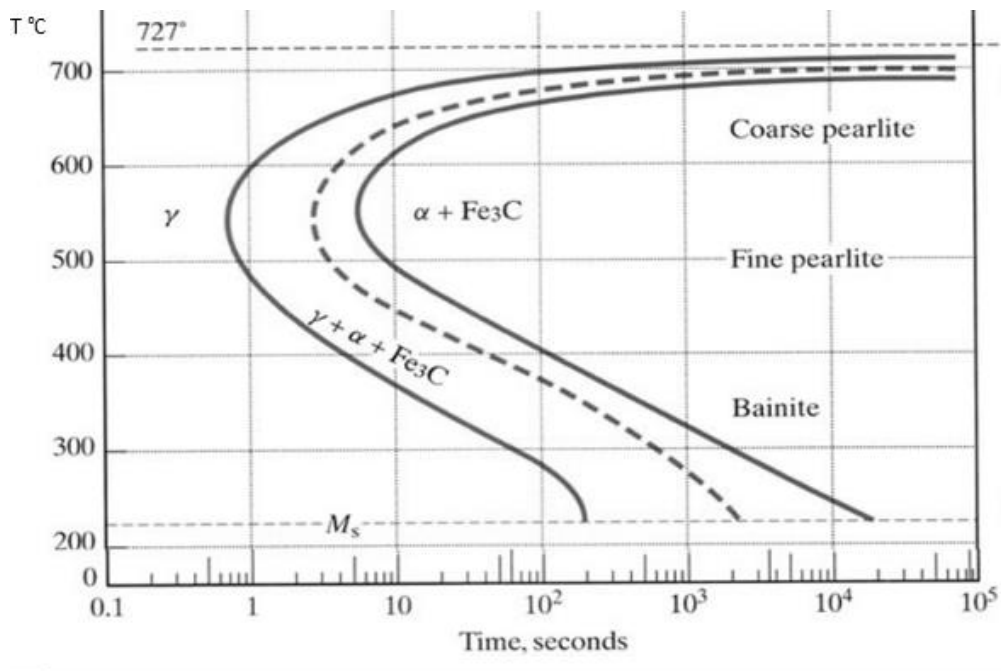


Figure 2.1 Schematic of time temperature transformation (TTT) for a high carbon steel (~0.8%C) (Charlie 1996)

However, the nanostructured bainitic steel is a high carbon (~0.8 wt. % C) and very low carbide steel due to its high Si content. To obtain nanostructured bainite, the steel is generally held at a temperature of 200 or 350 °C isothermally for different period of time and then air cooled (Garcia-Mateo et al. 2003). The structure of the steel is an interlace of retained austenite (enriched with carbon)

and bainitic ferrite laths region (depleted of carbon). The structure is basically 20 to 300 nm in thickness depending on the holding temperature (Timokhina et al. 2011). The fine feature of the bainitic structure is responsible for the superior mechanical properties (Caballero et al. 2007). The mechanical properties of the nanostructured bainitic steel (Table 2.1) shows that it has enhanced strength and its ductility is comparable to that of stainless steel and higher than that of martensitic steel.

**Table 2.1** Mechanical properties of common steels (Garcia-Mateo et al. 2003)

| Steel                  | Nanostructured bainitic steel | Martensitic steel | Stainless steel |
|------------------------|-------------------------------|-------------------|-----------------|
| Carbon %               | 0.8%C                         | 0.8%C             | 0.08%C          |
| Tensile strength (GPa) | 1.9-2.3                       | 0.9-1.6           | 0.5-0.8         |
| Ductility (%)          | 30                            | 10-25             | 12-40           |

For wide-spread applications of the nanostructured bainitic steel, it is be critical to evaluate its corrosion behaviour since steels in general, are susceptible to general and localised forms of corrosion.

### 2.3 Corrosion of Steel

Corrosion of steel is a serious world-wide problem. Its control can be expensive and the direct cost of corrosion in Australia has been estimated to be between A\$1-5 billion (CSIRO 2008) and about US\$ 160 per car annually for cars in USA (Finish Road Administration 1995). Corrosion can be defined as the deterioration of a material due to its reaction with the environment (Fontana 1987). Steels are in general prone to uniform and localised forms of corrosion and the process of corrosion is electrochemical in nature occurring at the interface between the metal

and an electrolyte solution. The deterioration or degradation of a material can be related to the rate of corrosion which is usually determined by an equilibrium between opposing electrochemical reactions i.e., the anodic (oxidation) and cathodic (reduction) reaction. The potential risk of corrosion can be unpredictable and may involve huge financial cost associated with shutdown of plants due to repairs/replacement or maintenance of corroded materials.

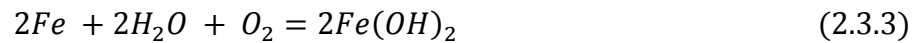
Generally, the anodic reaction involved in the corrosion of steel is shown in equation (2.3.1):



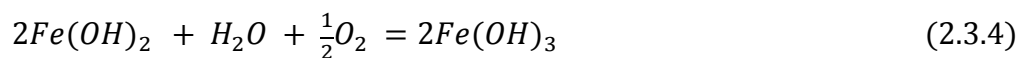
At the cathode oxygen is reduced into hydroxide ion shown in equation (2.3.2):



The overall reaction can be written as follows (2.3.3):



The corrosion product ferrous hydroxide is unstable and is further oxidized to ferric salt which is known as common rust: equation (2.3.4):



## 2.4 Types of Corrosion

Corrosion in metallic materials can be broadly classified into two types i.e., uniform and localized corrosion. The sections below describe the major sub classification of the forms of corrosion in engineering materials. The nanostructured bainitic steel may exhibit any or a combination of these forms of corrosion.

### ***2.4.1 Uniform Corrosion***

This type of corrosion is the most common and is readily detectable by visual inspection. It can be characterized by an even loss of metal from the entire corroding surface which can occur as a result of a chemical or electrochemical reaction. The result is a decreasing thickness of the corroded surface at a uniform rate which can thus be predictable over time. Therefore the rate of uniform corrosion may be expressed as a loss of thickness per unit time i.e., mm/year. The resistance to uniform corrosion is best provided by coating or alloying of the material.

### ***2.4.2 Localized Corrosion***

Corrosion in which there is an accelerated attack at localized sites on a material while the rest surface is not corroding or corroding at a much lower rate is classified as localized corrosion.

#### ***2.4.2.1 Pitting Corrosion***

It is one of the most damaging forms of localized corrosion which can result in small portions of metal dissolving out to produce pitting. Generally, pitting result from a small breakdown to a passive film or a coating layer locally while the rest of the surface remains intact. The process of corrosion may be galvanic in nature with the corroding area assuming anodic characteristic and the undamaged passive layer becomes the cathode. The rate of corrosion within the corroding region is usually rapid because the anode area is smaller compared to the cathode and as such may remain undetected or insignificant until the pitting eats deep and causes deep holes.

### 2.4.2.2 Galvanic Corrosion

Two dissimilar metals with different electrochemical potential will undergo galvanic corrosion in a conductive solution. The driving force for the corrosion is the potential difference between the two metals. Some factors such as the nature and aggressiveness of the corroding environment, distance and area effect have been shown to affect the rate of galvanic corrosion. The most appropriate method of preventing this form of corrosion is to select materials which in general are close together in the electromotive force (emf) series shown in (Table 2.2) to discourage a large potential difference. Secondly, avoid the unfavorable area effect of a small anodic site and large cathode or effectively create a barrier between the electrodes by coating or insulation.

**Table 2.2** Standard electromotive force (emf) series of metals (Fontana 1987)

|  | Metal-metal ion equilibrium (unit activity) | Electrode potential vs. normal Hydrogen electrode at 25°C, volts. |
|--|---|---|
| <br>Noble or cathodic | Au-Au <sup>+3</sup>                         | + 1.498   |
|  | Pt-Pt <sup>+2</sup>                         | + 1.2   |
|  | Pd-Pd <sup>+2</sup>                         | + 0.987   |
|  | Ag-Ag <sup>-</sup>                          | + 0.799   |
|  | Hg-Hg <sub>2</sub> <sup>+2</sup>            | + 0.788   |
|  | Cu-Cu <sup>+2</sup>                         | + 0.337   |
|  | H <sub>2</sub> -H <sup>+</sup>              | + 0.000   |
| Active or anodic<br>  | Pb-Pb <sup>+2</sup>                         | - 0.126   |
|  | Sn-Sn <sup>+2</sup>                         | - 0.136   |
|  | Ni-Ni <sup>+2</sup>                         | - 0.250   |
|  | Co-Co <sup>+2</sup>                         | - 0.277   |
|  | Cd-Cd <sup>+2</sup>                         | - 0.403   |
|  | Fe-Fe <sup>+2</sup>                         | - 0.440   |
|  | Cr-Cr <sup>+3</sup>                         | - 0.744   |
|  | Zn-Zn <sup>+2</sup>                         | - 0.763   |
|  | Al-Al <sup>+3</sup>                         | - 1.662   |
|  | Mg-Mg <sup>+2</sup>                         | - 2.363   |
|  | Na-Na <sup>+</sup>                          | - 2.714   |
| K-K <sup>+</sup>   | - 2.925                                     |   |

#### *2.4.2.3 Crevice Corrosion*

This type of corrosion occurs in confined spaces and cracks where supply of oxygen is restricted. The process or formation of crevice corrosion is initiated by a differential in aeration in which dissolved oxygen in the liquid medium in the crevice has been consumed by the reaction with the metal and further diffusion is limited. This results into the crevice area becoming more anodic as the metal dissolution in the crevice builds up. The surface which is more accessible to ambient air assumes the cathodic characteristics and as such initiates corrosion.

#### *2.4.2.4 Intergranular Corrosion*

Intergranular corrosion is a localized form of corrosion in which grain-boundaries are preferentially attacked with relatively little corrosion of the grains. The corrosion is initiated by the potential difference that exists between grain-boundaries and the grains caused by compositional differences or grain-boundary precipitate. This difference in corrosion potential between the grains and its boundaries causes a local cell to form. The corroded metal loses its strength and therefore is susceptible to failures. The best method to prevent intergranular corrosion is to eliminate the formation of intermetallic precipitate by solution heat treatment, lowering the content of alloying element prone to formation of precipitates and the addition of alloying elements that helps to stabilize the matrix.

#### *2.4.3 Stress Corrosion Cracking (SCC)*

SCC is caused by the simultaneous presence of tensile stress and a corrosive environment. The metal develops fine cracks as a result of corrosion and the cracks propagate deeper under tensile load. Often, the detection of this crack can be very difficult and damage may be unpredictable as the metal can fail at stress

below the yield stress. Certain material failures are caused by hydrogen. When hydrogen atom (produced from cathodic reactions) migrate and reside interstitially in the lattice of metals due to its much smaller size, it can greatly amplify the stress under applied load. This type of fracture is called hydrogen embrittlement. High strength steels are particularly susceptible to this type of failure and may require more treatment such as baking to remove hydrogen.

## **2.5 Corrosion Test Methods**

Immersion test and the electrochemical tests such as electrochemical impedance spectroscopy (EIS) and potentiodynamic polarisation are the popular test methods to evaluate the corrosion behaviour of metallic materials. Comparing the two tests, the electrochemical test methods provide more rapid information on the passivation and the corrosion mechanisms of material. In general, the corrosion test analysis forms the basis for the evaluation and selection of suitable materials, the suitability of the environmental, corrosion control and a data base for research purposes.

### ***2.5.1 Electrochemical Impedance Spectroscopy (EIS)***

EIS is a powerful method to understand the corrosion mechanism of metals. This method of corrosion testing provides a quick and most convenient evaluation of corrosion of metals and barrier properties of coating. It is a non-destructive technique that can be used to study the corrosion behavior of materials under a long-term exposure. This technique uses a small excitation of AC potential between 5 to 50 mV which is applied over a range of frequencies of 0.001 Hz to 100,000 Hz.

The response is an AC current signal which can be analyzed as sinusoidal function (Fourier series). The impedance equation can be expressed in term of Ohm's Law (equation 2.5.1) and represented thus (Gamry Instrument 2013):

$$Z = \frac{E_t}{I_t} = \frac{E_0 \sin(\omega t)}{I_0(\omega t + \varphi)} = Z_0 \frac{\sin(\omega t)}{\sin(\omega t + \varphi)} \quad (2.5.1)$$

where  $E_t$  is the potential at given time,  $E_0$  is the amplitude of the signal,  $\omega$  is the radial frequency,  $I_t$  is current at given time,  $I_0$  is current signal amplitude and  $\varphi$  is the phase shift between current and potential.

The equation is further simplified as

$$Z(\omega) = \frac{E}{I} = Z_0 \exp(j\varphi) = Z_0(\cos\varphi + j\sin\varphi) \quad (2.5.2)$$

The equation  $Z$  which composed of a real and an imaginary part can best be presented as a Nyquist Plot (Figure 2.2) with the real and imaginary part plotted as X-axis and Y-axis respectively. The Y-axis is plotted as negative and each value point is the impedance at one frequency. The Y-axis is plotted as negative and each value point is the impedance at one frequency. Furthermore, from the plot, low frequencies data are on the right side and the higher frequencies data are on the left. The Nyquist curves can usually be modeled and fitted with an equivalent circuit depending on the shape of the EIS spectrum. There is usually some basic assumption and adjustment to the circuit parameters until a best fitting spectrum is achieved. The quality of the fitting is judged by how well the fitting curve overlaps the original spectrum. By fitting the EIS data it is possible to obtain a set of parameters which can be correlated and be a representation of the electrochemical processes at the surface of the working electrode. The simplest

equivalent circuits that have been proposed to describe electrochemical interface is the Randle circuit.

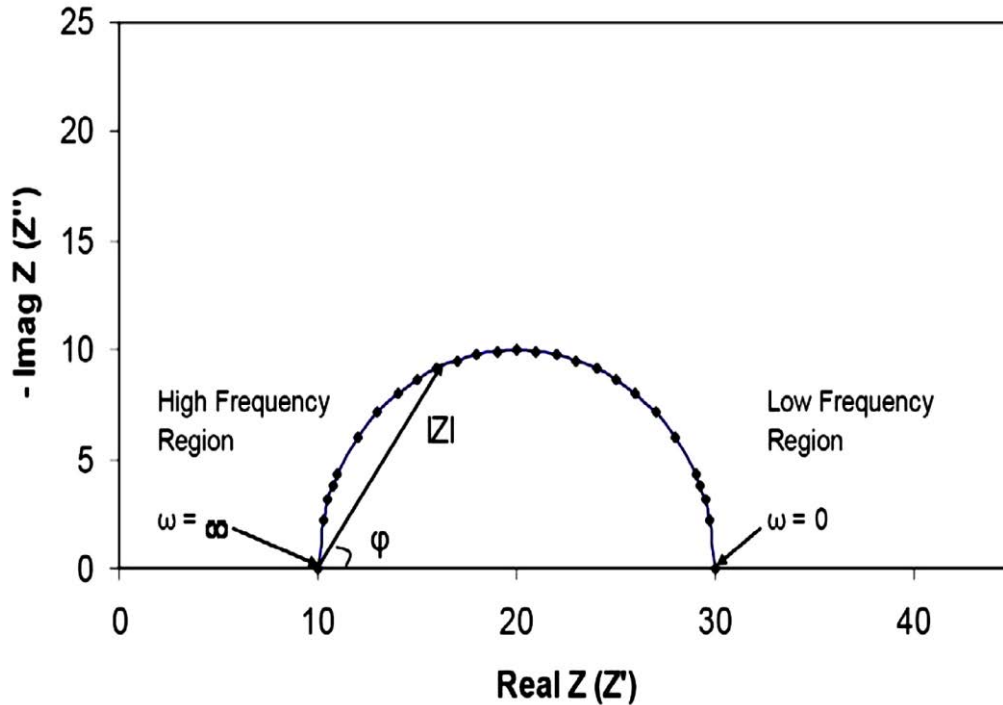


**Figure 2.2** A typical Nyquist plot (Parakala 2005)

### 2.5.2 Potentiodynamic Polarisation Method

Potentiodynamic polarisation is a commonly used technique to measure corrosion current  $i_{corr}$  and therefore the corrosion rate of metals. This technique provides significant information regarding the corrosion mechanisms of metals and corrosion resistance of material in a given corrosion environment. A typical polarisation technique involves changing the potential (E) by scanning through a range of values and the resultant induced current is recorded. The potential can be swept through the anodic direction (anodic polarisation) where metal oxidation is the dominant reaction taking place. Other relevant features such as passivation or oxygen evolution and pitting susceptibility may be presented on an anodic

polarisation curve. In the cathodic direction (cathodic polarisation) hydrogen evolution reaction becomes dominant. The combined scan is as shown in (Figure 2.3). The intersection of the corrosion potential ( $E_{corr}$ ) and the extrapolation of the Tafel region gives an estimation of the corrosion current density ( $i_{corr}$ ) and is proportional to corrosion rate  $CR$  from the following equation (www.gamry.com, Yang 2008, Srikanth et al. 2007):

$$CR = \frac{3.27 \times 10^{-3} i_{corr}.EW}{D} \quad (2.2.3)$$

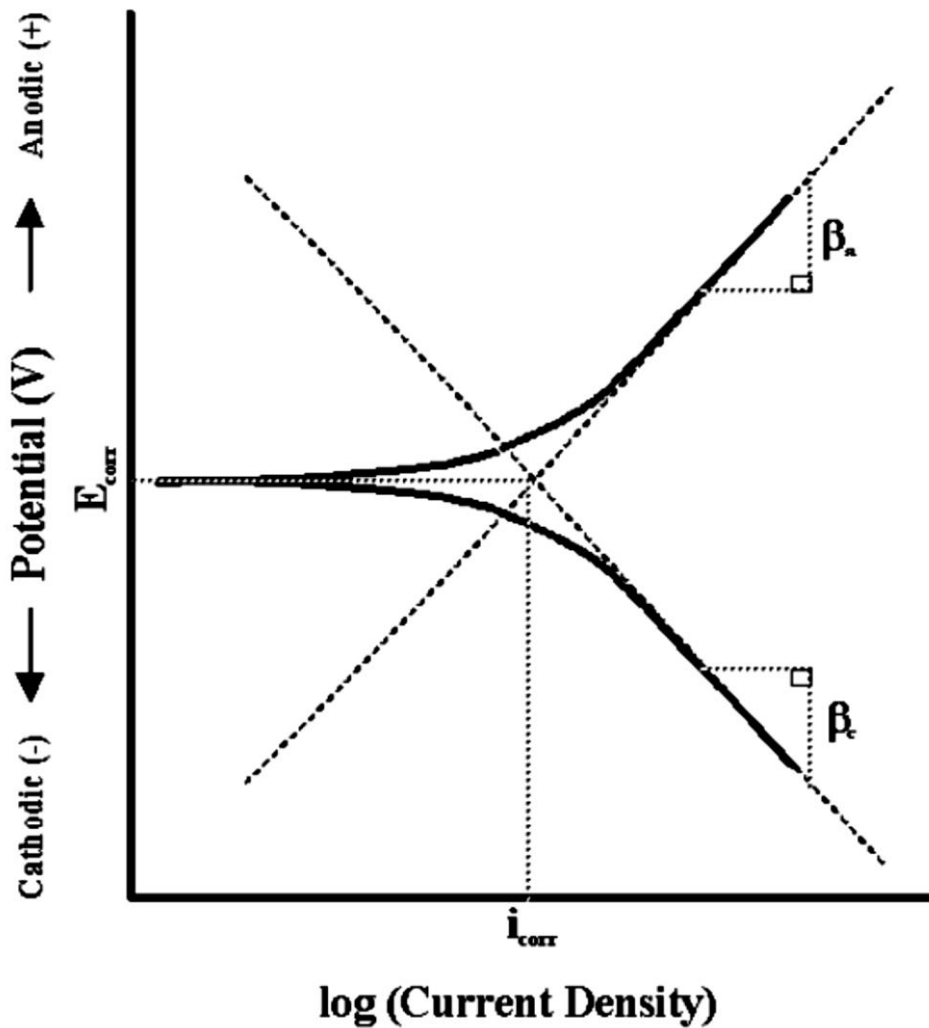


Figure 2.3 A typical potentiodynamic polarisation scan

where  $CR$  is corrosion rate in mm/year,  $i_{corr}$  the corrosion current density ( $A/cm^2$ ),  $EW$  is equivalent weight and  $D$  = the density of the metal in  $g/cm^3$ .

## **2.6 Corrosion Mechanisms: Effect of Microstructure**

It is well known that microstructural phase constituent can affect both the mechanical properties and corrosion behavior of steels. Generally, Steels have various alloying elements such as carbon (C), silicon (Si), manganese (Mn), aluminum (Al), chromium (Cr), cobalt (Co) and molybdenum (Mo). These elements influence materials differently when they form oxide films or precipitates. For example, C is added to iron to improve the strength of steel. The typical iron-iron-carbide phase diagram (Figure 2.4) shows increasing cementite precipitation for high carbon steel during heat treatment. Cementite is known to influence corrosion resistance of steel (Pereloma et al. 2007). Si addition mainly improves corrosion resistance and suppresses the formation of carbide in carbon rich steel. Si in excess of 0.6 wt. % dissolves in ferrite. Other elements such as Cr essentially improve corrosion resistance when added in excess of 12 wt. % by forming protective oxide. Ni can be added to promote the austenitic structures and Ni in increasing amount improves toughness. Mn is an inexpensive alloying element added to steel as a deoxidizer. It is a weak carbide former and is effective only in excess of 0.8 wt. % as a hardener, but at a lesser degree than carbon. On the other hand, Mo has increased high-temperature hardness of steel. High strength in steel is desirable due to improved weight to strength ratio. This translates therefore to a lower material cost and higher loading and impact resistance over the traditional mild steel. However, corrosion resistant steel are equally important. A high carbon steel can be transformed to a high strength steel with three different microstructure. This can be done by quenching from high

temperature to form martensite or slowly cooled to form upper or lower bainite. The interaction of the carbon with other alloying elements can cause redistribution, refinement of different phases or influence the volume fraction of each phase (Caballero et al. 2004) and hence the corrosion behaviour.

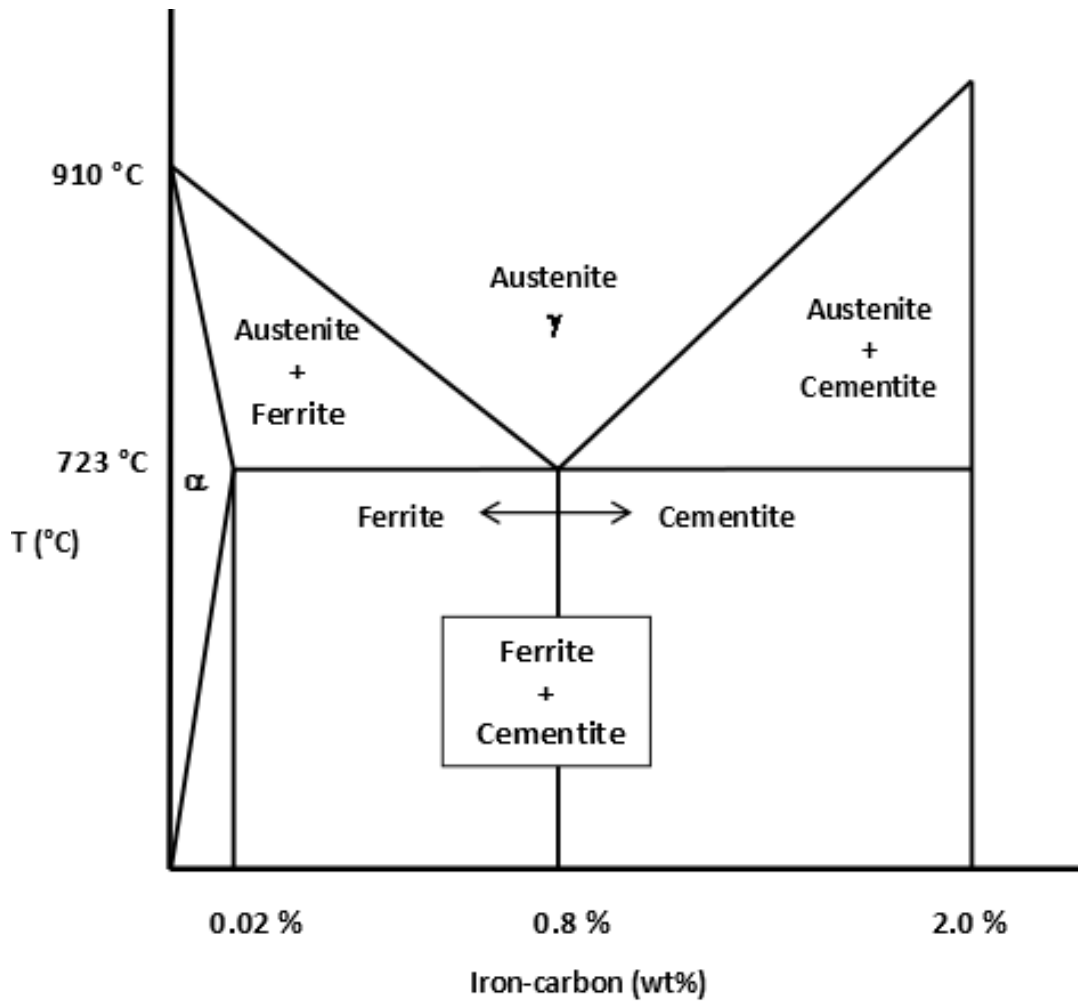


**Figure 2.4** Schematic of iron-iron carbide phase diagram

Therefore, it is critical to understand the localised and general form of corrosion behaviour of nanostructured bainitic steel. A summary of literature as shown in Table 2.3 suggest that the morphology of corrosion can be related to the microstructural composition of the phases in steel materials. For instance, for duplex steel, the austenite phase appears to be more susceptible to corrosion

attack than the ferrite phase. However, either phase can be selectively corroded depending on the chemical composition and the volume of the individual phase in the steel.

## **2.7 Corrosion Protection: Conducting Polymers**

Surface coating has been a popular method for the protection of metallic materials against corrosion. The use of conducting polymers has increasingly generated interest in the protection of metals against corrosion, due to their high electrical conductivity which is particularly useful in inhibiting corrosion (Casalheira et al. 2003). A summary of literatures on the performance of conducting polymers is as shown in (Table 2.4). The corrosion protection properties of conducting polymers have been described by two mechanisms: the barrier effect and the redox performance at the metal polymer interface (Wessling 1997; Camalet et al. 2000). The synthesis of the polymer can be done either chemically or electrochemically. The chemical deposition (Yao et al. 2008) is obtained by oxidation from an aqueous solution of an acid-polymer blend and the coating is therefore dependent on the composition of the acid, nature of the oxidant, rate of oxidation, temperature and pH of the solution (Martyak et al. 2002; Wessling 1994). In recent years, electrochemical technique is widely used due to its simpler process and the direct synthesis of coating on the metal surface without any organic additives (Kraljic et al. 2003). Nevertheless, the synthesis of conducting polymer on oxidizable metal has posed a challenge due to the prior dissolution of the substrate. The metal dissolution was reportedly responsible for inhibiting the oxidation reaction (Guvzddenovic et al. 2011) and therefore the prevention of an adherent polymer coating on the substrate. Past studies done typically used mineral acids such as HCl and H<sub>2</sub>SO<sub>4</sub> as solvent and supporting electrolyte,

although much of the successful synthesis now employ the use of neutral aqueous media such as oxalic acid and sodium salicylate (Camalet et al. 2000; Gvozdenovic et al. 2011; Petitjean et al. 1999). Such neutral aqueous electrolytes were reported to reduce substrate dissolution and passivate the substrate which was shown to be a necessary step for the formation of an adherent coating (Camalet et al 1996).

Polyaniline (PANI) and polypyrrole (PPy) are among the widely used conducting polymer for corrosion inhibition (Herrasti and Ocon 2001; Martins et al. 2004; Pawar et al. 2006; El-Shazly and Turaif 2012). PANI has been widely studied as a most promising polymer for corrosion protection. Report suggests it can provide corrosion protection on metal in acidic and neutral environment (Martins et al. 2002). Their synthesis on metals has been reported to have enhanced corrosion protection of several metallic materials. Studies have also shown that corrosion protection offered by these polymers on metals such as mild steel, aluminum, copper and zinc coated steel (Patil et al. 2004; Shinde et al. 2005; Aeiyaich et al. 1999; Saidman and Bessone 2002; Ogurtsov et al. 2004) can be attributable to the passivation of the metal surface by the redox property of the polymer (Zhou et al. 2004; Tuken et al. 2006; Wessling 1997). The passive film was reported to be effective for corrosion protection on metals even when minor defects and pinholes were present (Kinlen et al. 1997). The performances of the coating depended on the coating techniques, processing conditions (Zhou et al. 2006) and the type of metallic substrate used (Herrasti and Ocon 2001; Martins et al. 2002). Some of the electrochemical techniques available include cyclic voltammetry, potentiostatic and galvanostatic (Kraljic et al. 2003; Martins et al. 2004) methods however, the galvanostatic technique is becoming more suitable due to its one step process.

Varying the coating parameters have shown that the coating thickness can be increased (Tuken et al. 2006). The increase in thickness is suggested to improve the barrier between the substrate and corroding environment. While galvanostatic synthesis has been reported to be effective in producing thick films in a short time at higher current density (Martins et al. 2002), there arises an issue of high bubble formation which can affect the coating performance. Therefore, the corrosion performance of the coating can be dependent on a number of factors. While much work has been done on steel with low carbon content, this study investigates the performance of the high carbon steel coated with PANI using galvanostatic techniques in a chloride-containing environment.

**Table 2.3** Summary of literature on corrosion of steels

| Material                     | Electrolyte  | Test Methods                                    | Observation  | Reference                |
|------------------------------|--|---|--|--------------------------|
| Aged duplex stainless steel  | 5 wt.% HCl solution  | Immersion test                                  | Selective dissolution of ferrite   | Yi et al. 1996           |
| High chromium steel          | 3 M HCl and LiCl   | Electrochemical polarisation                    | Austenite corrodes due to nitrogen content in ferrite                                | Perren et al. 2001       |
| 304 Stainless steel          | HCl and HF   | Immersion test                                  | Intergranular corrosion was evident  | Lian et al. 2004         |
| Dual-phase martensitic steel | 3.5 wt.% NaCl solution                                     | Galvanostatic polarization                      | Martensitic phase more susceptible to corrosion                                      | Sarkar et al. 2005       |
| Austenitic stainless steel   | 2 M H <sub>2</sub> SO <sub>4</sub> and 0.5 M NaCl solution | Immersion and potentiokinetic reactivation test | Intergranular corrosion was observed   | Terada et al. 2006       |
| Low carbon steel             | 3.5 wt.% NaCl  | Immersion and EIS                               | Ferrite structure corrosion observed   | Zhao et al. 2007         |
| Duplex steel with Ni content | 3.5 wt.% NaCl  | Potentiodynamic polarization technique          | Austenite phase corrosion observed   | Potgieter et al. 2008    |
| Austenitic steel             | 3.5 wt.% NaCl  | Potentiodynamic polarization technique          | Corrosion increases with carbide formation   | Tuan et al. 2009         |
| Duplex stain less steel      | 3.5 wt.% NaCl in bacterial media                           | Potentiodynamic polarization technique          | Austenite more susceptible, but with heat treatment –ferrite become more susceptible | Antony et al. 2010       |
| Duplex stainless steel       | Ferric chloride test                                       | Immersion test                                  | Austenite corrodes, reversible by addition of Ni                                     | Da-wei et al. 2012       |
| Duplex steel                 | 10 % Oxalic acid   | Etch electrochemically                          | Selective corrosion of austenite, reversible to ferrite by thermal aging             | Della-Rovere et al. 2013 |

**Table 2.4** Summary of literature on corrosion prevention by using conducting polymers

| Material                | Coating | Test Methods                                 | Observation  | Reference               |
|-------------------------|---------|--|--|-------------------------|
| Iron, steel and copper  | PANI    | Optical evaluation                           | High corrosion protection by redox properties  | Wessling et al. 1997    |
| Steel                   | PANI    | Immersion test                               | Corrosion protection enhanced significantly  | Kinlen et al. 1997      |
| Steel, aluminium        | PANI    | General review                               | Protection enhanced  | Sitaram et al. 1997     |
| Zinc, mild steel        | PPy     | Cyclic voltammetry and galvanostatic methods | Passivation and corrosion enhancement and adherence 100%, growth of coating was $1 \mu\text{m s}^{-1}$ | Petitjean et al. 1999   |
| Mild steel              | PANI    | Cyclic voltammetry and galvanostatic methods | Corrosion protection observed and adhesion was good  | Camalet et al. 2000     |
| Steel                   | PANI    | Cyclic voltammetry method                    | Good adhesion if scan was reversed   | Martyak et al. 2002     |
| Iron and steel          | PPy     | Galvanostatic and potentiodynamic methods    | Galvanostatic technique showed good adhesion (100%)  | Martins et al. 2002     |
| Copper                  | PPy     | Galvanostatic and potentiostatic methods     | Homogeneous, uniform films produced but poor adhesion observed under potentiostatic method             | Cascalheira et al. 2003 |
| Zinc coated steel       | PPy     | Salt spray test and DC polarization test     | Ultrasound enhances coating performance  | Martins et al. 2004     |
| Aluminium alloy Al 3003 | PANI    | Electrochemical test                         | Corrosion protections enhanced in neutral and dilute acidic solution                                   | Ogurtsov et al. 2004    |
| Stainless steel         | PANI    | Pulse galvanostatic method                   | Nano-fibular PANI films observed   | Zhou et al. 2004        |
| Mild steel              | PPy     | EIS, anodic polarization                     | Corrosion protection enhanced in long term test  | Tuken et al. 2006       |

---

|                 |                             |   |   |                         |
|-----------------|-----------------------------|---|---|-------------------------|
| Copper          | Poly ( <i>o</i> -anisidine) | Potentiodynamic polarization test                 | Corrosion protection enhanced by two orders of magnitude  | Chaudhari et al. 2006   |
| Mild steel      | PANI                        | EIS and potentiodynamic polarization              | High corrosion protection, uniform and good adherent coating                                      | Pawar et al. 2006       |
| Steel           | PANI                        | Interfacial and chemical oxidative polymerization | High corrosion protection observed with PANI nanofibres synthesised by interfacial polymerisation | Yao et al. 2008         |
| Copper          | PPy                         | Cyclic voltammetry and potentiostatic methods     | Non uniform coating due to reduction of previously formed passive layer                           | Cascalheira et al. 2003 |
| Stainless steel | PPy                         | Constant potential method                         | Coating time enhance coating performance  | Subathira et al. 2010   |
| Steel           | PANI                        | Potentiodynamic polarization test                 | Enhanced corrosion protection by a factor of 1.88 in common environment                           | El-Shazly et al. 2012   |
| -               | PANI                        | Review  | Corrosion protection interpreted in terms of barrier and anodic protection mechanism              | Gvozdenovic et al. 2012 |

---

## CHAPTER 3: MATERIALS AND EXPERIMENTAL PROCEDURE

### 3.1 Material Characterization

#### 3.1.1 Material and Heat treatment

The chemical composition of the steel used in this study is shown in Table 3.1. To produce the nanostructured bainitic microstructure, the steel was initially heated to 1100 °C and held for 30 min in a muffle furnace.

**Table 3.1** Chemical composition of the steel used in this study

| Elements | C    | Si  | Mn   | Cr   | Mo   | Al   | Co   | Fe  |
|----------|------|-----|------|------|------|------|------|-----|
| Weight % | 0.79 | 1.5 | 1.98 | 0.98 | 0.24 | 1.06 | 1.58 | Bal |

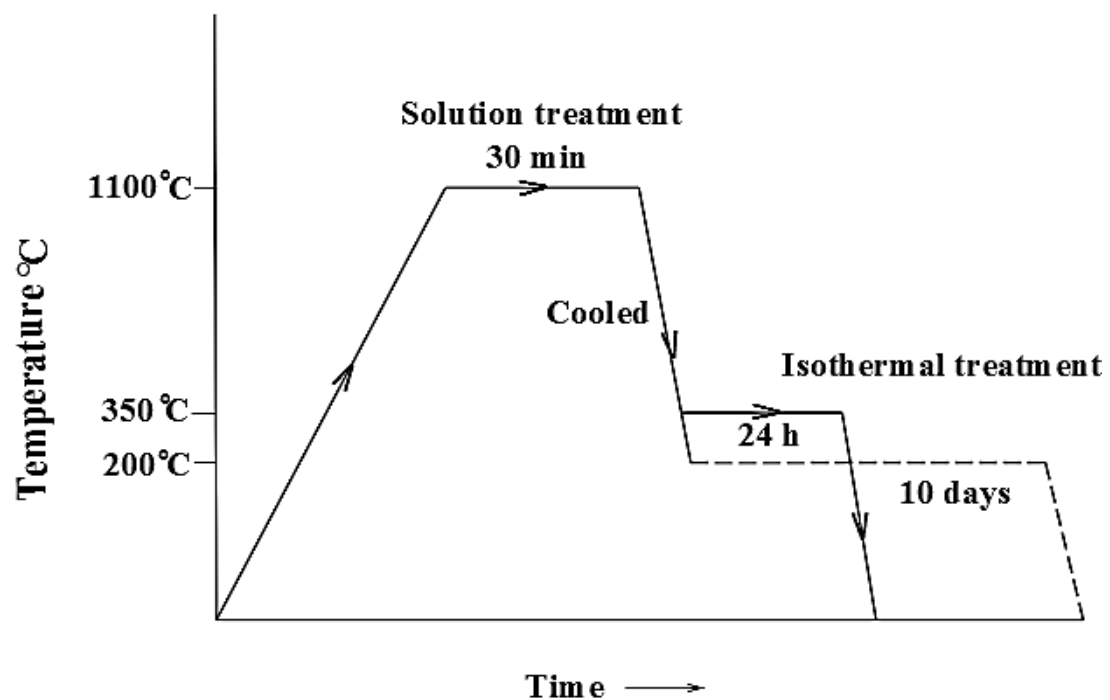


**Figure 3.1** Heat treatment procedure used to produce nanostructured bainitic steel

The samples were then placed in a salt bath furnace at 200 °C for 10 days or 350 °C for 24 h followed by air cooling to produce two different nanostructured bainitic steels as described elsewhere (Timokhina et al. 2011). For comparison martensitic steel having the same chemical composition as the nanostructured bainitic steel was formed by air-cooling the steel after austenizing at 1100 °C for 30 min (Figure 3.1).

### ***3.1.2 Microstructure Analysis***

The microstructures of the steel after the different heat-treatments were analysed using transmission electron microscopy (TEM) along with X-ray diffraction technique. Disc-shaped TEM foils 3 mm in diameter were mechanically ground to a thickness of about 70 µm and then twin-jet electropolished using a solution containing 5% perchloric acid and 95% methanol at a temperature of 25 °C and a voltage of 50 V. TEM examination of thin foils was performed using a Philips CM-20 microscope operated at 200 kV. X-ray diffraction (XRD) analysis was also performed using a Philips PW 1130 (40 kV, 25 mA) diffractometer to calculate the amount of retained austenite.

### ***3.1.3 Test Samples Preparation***

The test samples (size ~20 mm × 20 mm × 2 mm) were mounted on teflon resin and a typical metallographic preparation method was followed. The samples were ground with SiC papers up to 2500 grit followed by alumina polishing. They were cleaned by ultrasonic cleaning in acetone and ethanol prior to use for corrosion performance evaluation. All tests were conducted in triplicate to confirm the reproducibility.

### 3.2 Electrochemical Corrosion Testing

Electrochemical impedance spectroscopy (EIS), potentiodynamic polarization and galvanostatic polarisation techniques were used to evaluate the electrochemical corrosion behavior of the samples. A typical three-electrode system as shown in Figure 3.2 was used in this study, i.e., graphite rod (A) as counter electrode, silver/silver-chloride (Ag/AgCl) as the reference electrode (B), sample as a working electrode (C). The electrolyte (D) is 3.5 wt.% NaCl solution was used in the study. The cell setup was connected to a potentiostat (Model: VersaSTAT3 PAR).

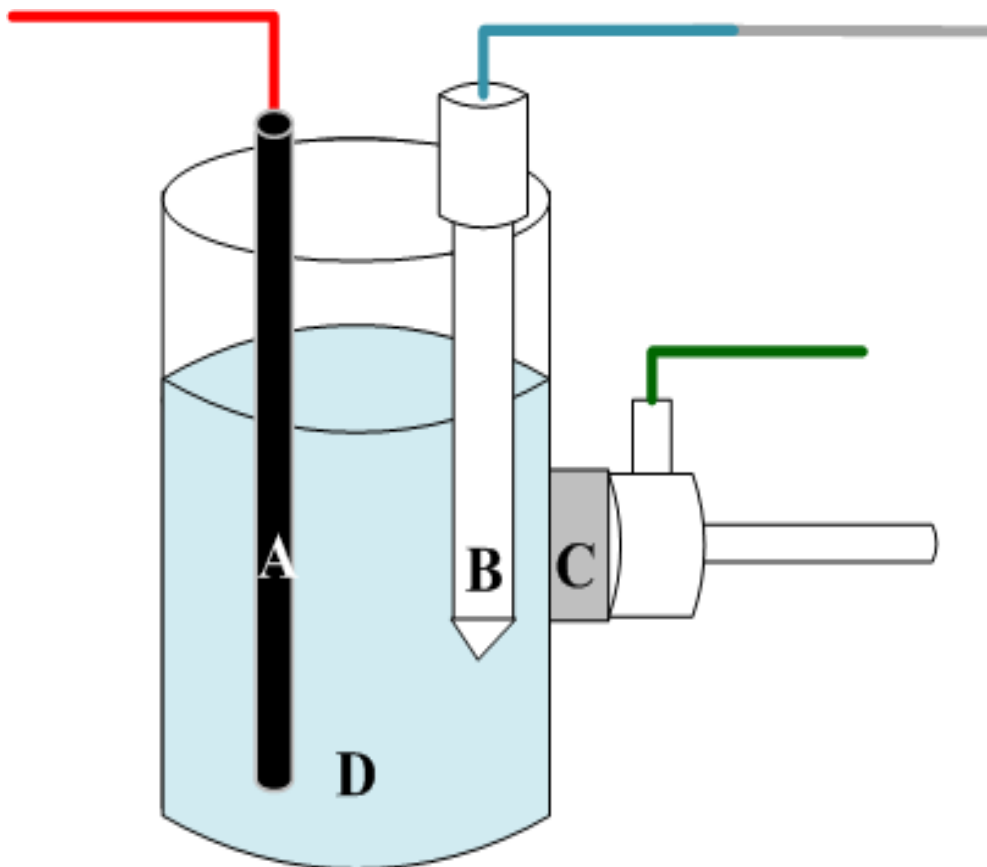


**Figure 3.2** Schematic of the three-electrode cell used for electrochemical experiment (*Note: A: counter electrode, B: reference electrode, C: working electrode and D: electrolyte*)

EIS experiments were performed at open circuit potential with an AC amplitude of 5 mV over the frequency range of  $10^5$  Hz to  $10^{-2}$  Hz. Potentiodynamic polarisation experiments were carried out at a scan rate of 0.5 mV/s. Prior to the EIS and polarisation experiments the samples were kept immersed in the electrolyte for 1 h to establish the free corrosion potential. Galvanostatic polarisation was carried out by imposing a constant current density of  $10 \text{ mA/cm}^2$  on the samples for 1 h. Long term immersion test were carried out in 3.5 wt.% NaCl solution. The EIS spectra were modelled using ZsimpWin 3.2.1 software. The post corrosion analysis was carried out using a scanning electron microscopy (SEM) Model : Jeol JSM 530LV to identify the mode of corrosion attack.

### **3.3 Electrochemical Coating**

Electrochemical polymerisation using galvanostatic technique was used to coat aniline on steel. The electrolyte used in the coating process contained 0.3 M aniline and 0.1 M aqueous sodium salicylate prepared in distilled water.

#### ***3.3.1 Galvanostatic Technique***

The galvanostatic coating was carried out using current density between 1 to 20  $\text{mA cm}^{-2}$  connected to a VersaSTAT3 PAR potentiostat. The mounted samples were immersed in the coating medium in a three-electrode cell. The duration of coating was also changed to form coated samples with different thickness. Two different bath conditions were investigated: (i) unstirred and (ii) stirred conditions at 600 rpm (using a magnetic stirrer) at a constant current density of  $20 \text{ mA cm}^{-2}$  for 20 min.

### ***3.3.2 Coating Characterization***

The uniformity of the coatings was examined using (SEM). A thickness gauge (Model: Dual Scope) was used to measure the coating thickness. The adhesion of the coatings was measured using an adhesion tester (Model: Elcometer 106) and Fourier transform infrared spectroscopy (FTIR) analysis of the coatings was recorded in a spectral range of 1800-500  $\text{cm}^{-1}$  using a spectrometer (Model: Perkin Elmer spectrum 100). The coating performance on steel was then investigated using the electrochemical impedance spectroscopy (EIS) and potentiodynamic polarisation test as detailed in section 3.2.

## CHAPTER 4: CORROSION BEHAVIOUR OF NANOSTRUCTURED BAINITIC STEEL

### 4.1 Aqueous Corrosion Behaviour

In order to evaluate the corrosion behaviour of nanostructured bainitic steel in an aqueous environment, electrochemical techniques were used. For comparison, a martensitic steel of the same composition was also studied.

#### 4.1.1 Microstructure

Generally the corrosion behavior of metals is influenced by their microstructures. Hence, it is critical to study the microstructure the nanostructured bainitic steel. The TEM micrographs of the nanostructured bainitic steel are shown in Figure 4.1. The dominant features are nanolayers of bainitic ferrite ( $\sim 60 \pm 10$  nm thickness) and retained austenite ( $\sim 30 \pm 5$  nm). The volume fraction of the retained austenite was  $\sim 21 \pm 2$  %.

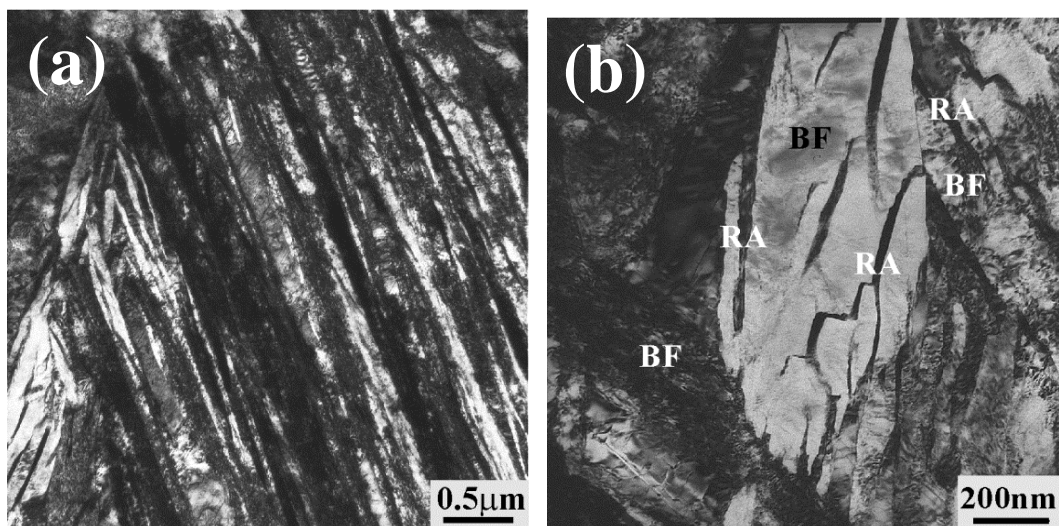


**Figure 4.1** TEM micrographs of nanostructured bainitic steel (a) low magnification and (b) high magnification (*note: RA is retained austenite and BF is bainitic ferrite*)

Literature revealed enrichment of carbon in the retained austenite and the detailed analysis of the structure of the nanostructured bainitic steel can be found elsewhere (Timokhina et al. 2011).

#### 4.1.2 Open Circuit Potential

The open circuit potential (OCP) plots for nanostructured bainitic steel and martensitic steel are shown in Figure 4.2. The electrochemical potential of both the steel samples decreased with exposure time, which suggests active corrosion. However, the steepness in the curve was higher for martensitic steel as compared to nanostructured bainitic steel. The potential difference between the steel samples was more than 100 mV after 1 h exposure in chloride-containing solution, and the potential of the martensitic steel was nobler than that of the nanostructured bainitic steel.

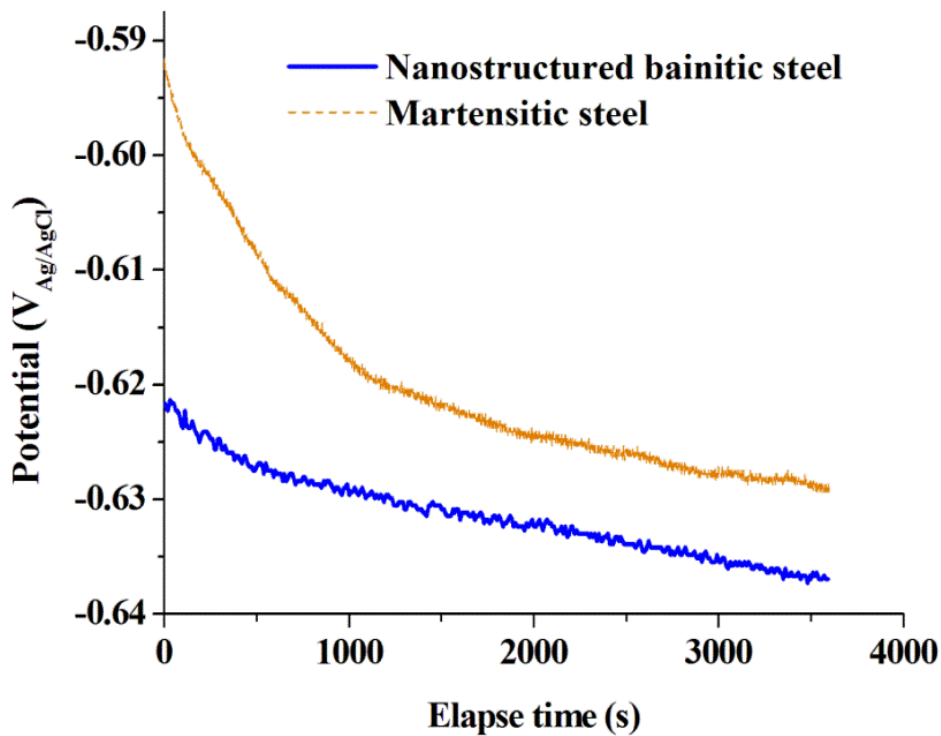


**Figure 4.2** Open circuit potential (OCP) curves for nanostructured bainitic steel and martensitic steel in 3.5 wt. % NaCl solution

#### 4.1.3 Electrochemical Impedance Spectroscopy (EIS)

Figure 4.3 shows the Nyquist plots of the nanostructured bainite steel and the martensitic steel. The equivalent circuit used for modelling the Nyquist plots consist of electrolyte resistance ( $R_s$ ), film resistance due to corrosion layer ( $R_f$ ), film capacitance ( $C_f$ ), charge-transfer resistance ( $R_{ct}$ ) and double layer capacitance ( $C_{dl}$ ) (Guo et al. 2008; Bordbar et al. 2013).

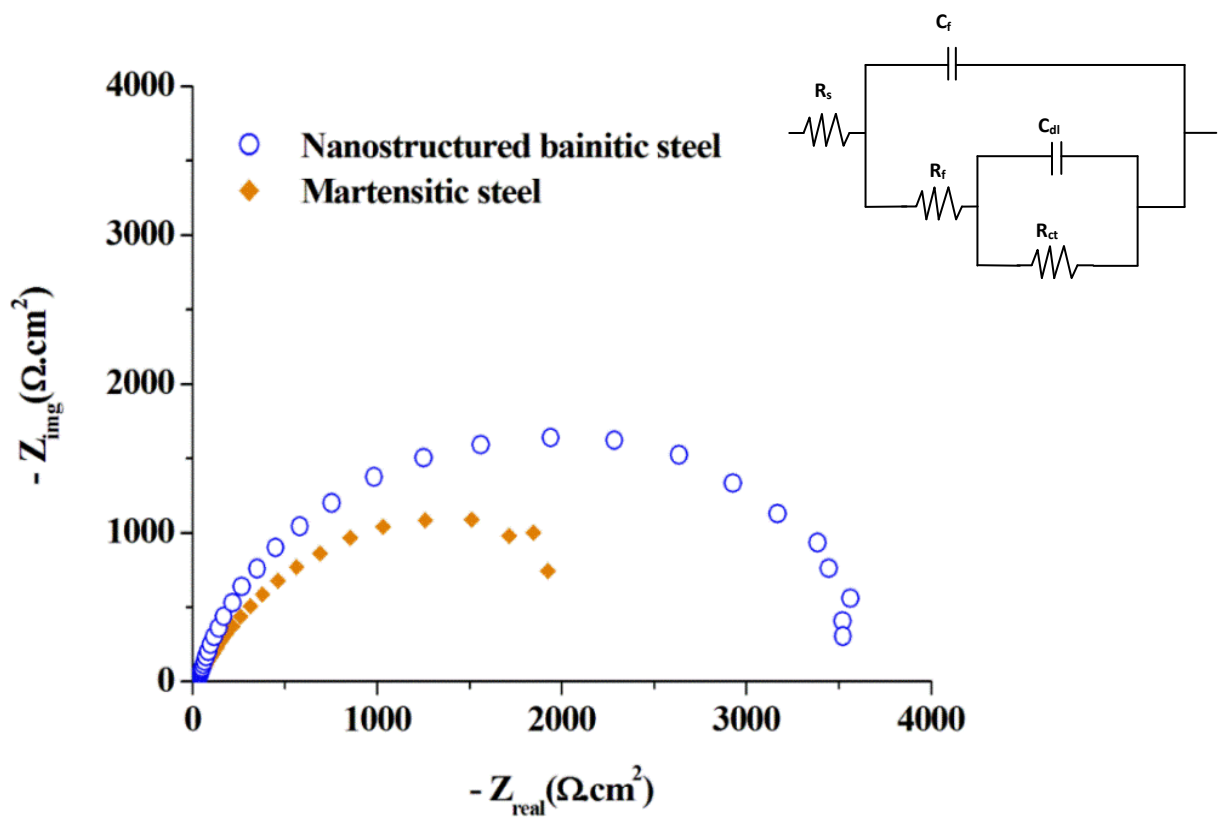


**Figure 4.3** Nyquist plots of nanostructured bainitic steel and martensitic steel exposed to 3.5 wt.% NaCl solution

The polarisation resistance ( $R_p$ ) of the samples was calculated by adding  $R_{ct}$  and  $R_f$ . The EIS data obtained from the equivalent circuit modelling is given in Table 4.1. The nanostructured bainitic steel exhibited an  $R_p$  of  $3400 \Omega \text{ cm}^2$  and the martensitic steel showed an  $R_p$  of  $2000 \Omega \text{ cm}^2$ . The  $R_p$  value of nanostructured bainitic steel was higher by 70% than that of the martensitic steel. The difference

in the  $R_p$  values is significant to suggest that nanostructured bainitic steel possesses higher corrosion resistance than the martensitic steel.

**Table 4.1** EIS data obtained from equivalent circuit modelling of the impedance spectra

|                       | Nanostructured bainitic steel   | Martensitic steel               |
|-----------------------|---------------------------------|---------------------------------|
| $R_s(\Omega.cm^2)$    | 26                              | 23                              |
| $R_f(\Omega.cm^2)$    | 260                             | 150                             |
| $C_f(F/cm^2)$         | $4.364 \times 10^{-5} \pm 0.11$ | $1.359 \times 10^{-4} \pm 0.22$ |
| $R_{ct}(\Omega.cm^2)$ | $3100 \pm 30$                   | $1850 \pm 20$                   |
| $C_{dl}(F/cm^2)$      | $6.342 \times 10^{-5} \pm 0.23$ | $1.449 \times 10^{-4} \pm 0.12$ |
| $R_p(\Omega.cm^2)$    | $3400 \pm 30$                   | $2000 \pm 20$                   |

#### 4.1.4 Potentiodynamic Polarisation

The potentiodynamic polarisation curves of both the steel samples in chloride-containing solution are shown in Figure 4.4 and the corresponding parameters are given in Table 4.2. Based on the OCP curves (Figure 4.2), it was expected that the corrosion potential ( $E_{corr}$ ) of the martensitic steel will be nobler to the nanostructured bainitic steel. The cathodic curves of both the steel samples suggest that the cathodic reaction is a diffusion controlled process, i.e. oxygen reduction reaction ( $O_2 + 4H^+ + 4e^- \rightarrow 2H_2O$ ). It can be noted that the cathodic current for nanostructured bainitic steel is significantly lower than the martensitic steel. Interestingly, the martensitic steel showed a slightly lower current than the nanostructured bainite at potentials close the OCP. However, increase in potential towards the noble direction decreased the difference in the current between the

two steel samples. The corrosion current density ( $i_{corr}$ ) calculated based on the cathodic and anodic curves showed that the  $i_{corr}$  of nanostructured bainitic steels was lower by 85% than the martensitic steel.

The nanostructured bainitic steel and martensitic steel exhibited  $i_{corr}$  of  $0.776 \pm 0.40 \mu\text{A}/\text{cm}^2$  and  $5.370 \pm 0.47 \mu\text{A}/\text{cm}^2$  respectively.

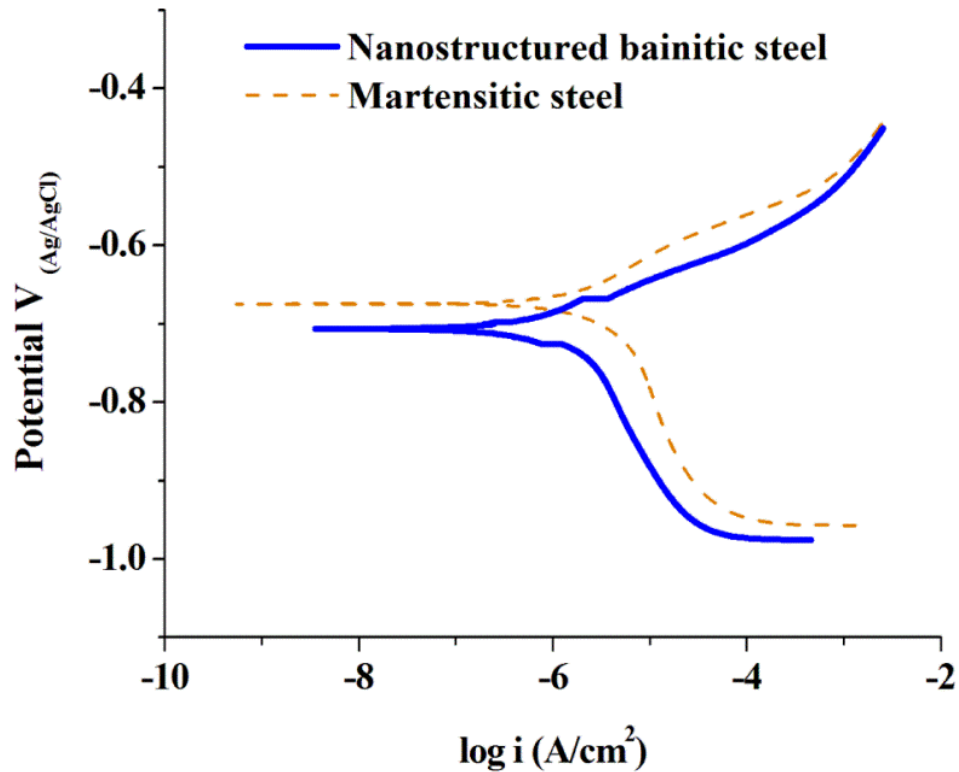


**Figure 4.4** Potentiodynamic polarization plots for the nanostructured bainitic steel and martensitic steel in 3.5 wt. % NaCl solution

**Table 4.2** Potentiodynamic polarisation data of the nanostructured bainitic steel and the martensitic steel in 3.5 wt. % NaCl solution

|   | Nanostructured bainitic steel | Martensitic steel  |
|---|-------------------------------|--------------------|
| $i_{corr} (\mu\text{A}/\text{cm}^2)$          | $0.776 \pm 0.40$              | $5.370 \pm 0.47$   |
| $E_{corr} (\text{V}_{\text{Ag}/\text{AgCl}})$ | $-0.706 \pm 0.011$            | $-0.662 \pm 0.021$ |

#### 4.1.5 Post-Corrosion Analysis

Post-corrosion SEM micrographs of the galvanostatically polarised nanostructured bainitic steel and martensitic steel are shown in Figure 4.5. The nanostructured bainitic steel exhibited general corrosion, but a closer look at the attacked region revealed a pattern of selective dissolution. In the case of martensitic steel, the corrosion attack was highly localized, i.e., the corrosion attack was predominantly along the grain boundaries leading to a typical intergranular corrosion (IGC). Localized attack in the grains was also observed in the martensitic steel.

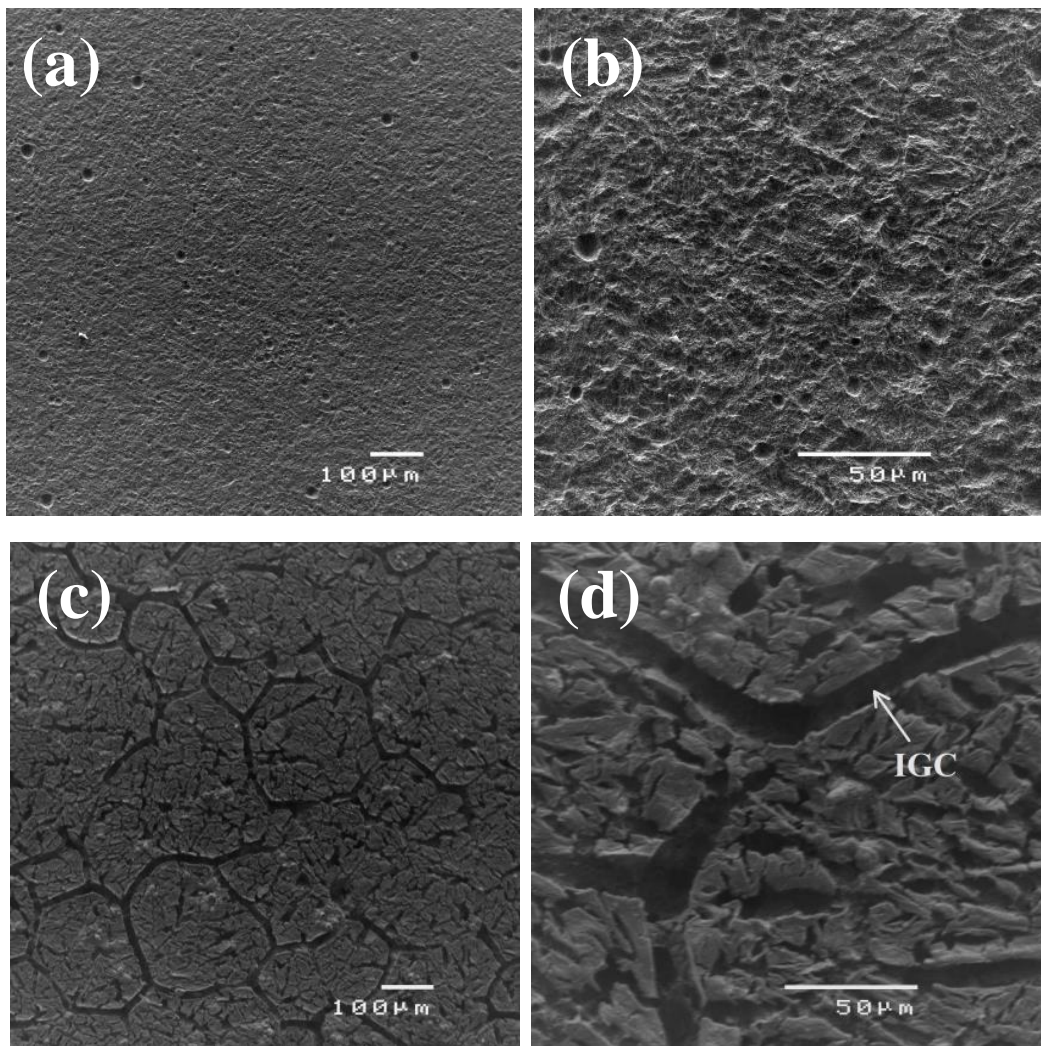


**Figure 4.5** SEM micrographs of galvanostatically polarised samples in 3.5 wt. % NaCl solution: (a and b) nanostructured bainitic steel (c and d) martensitic steel

In order to understand the morphology of the corrosion products, long-term immersion tests, i.e., 7 days exposure in 3.5 wt. % NaCl solution were carried out for both the steel samples. Figure 4.6 shows the post-corrosion SEM micrographs of the steels with the corrosion products. It is clear evident that the amount of corrosion products formed on nanostructured bainitic steel is significantly lower than that of martensitic steel, which confirms the better performance of nanostructured bainitic steel. Although the two steel samples have the same chemical composition, they exhibited different modes and degree of corrosion. This can be attributed to the difference in the microstructure of the steel samples.

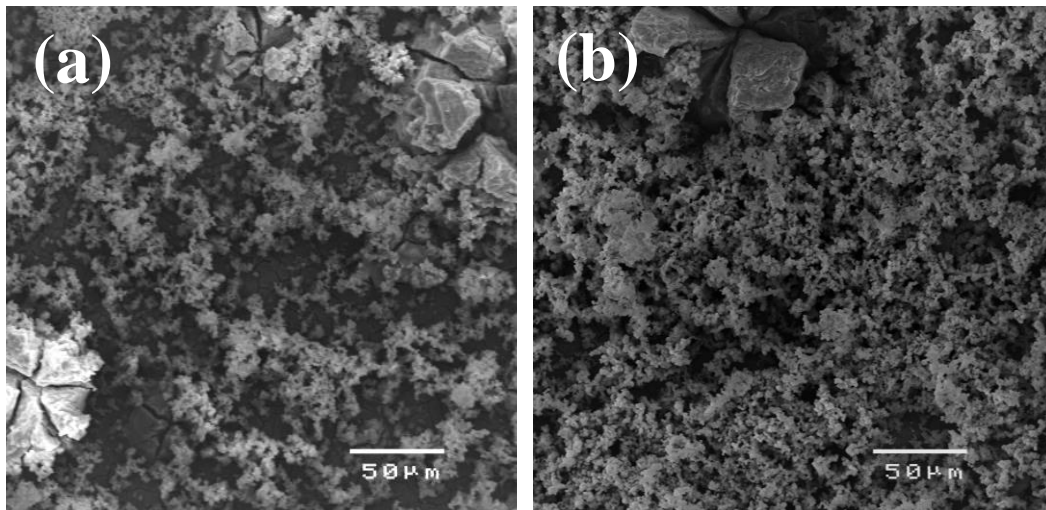


**Figure 4.6** SEM micrographs of samples immersed in 3.5 wt. % NaCl solution for 7 days: (a) nanostructured bainitic steel, and (b) martensitic steel

A schematic representation of the microstructures of both the steels before and after corrosion is shown in Figure 4.7. In the nanostructured bainitic steel, a selective dissolution pattern was evident when observed closely. Literature suggested that the carbon distribution in the retained austenite is higher than in the bainitic ferrite (Timokhina et al. 2011; Tehovnik et al. 2011) and the high Si

content discourages formation of carbides in the ferrite (Timokhina et al. 2011). Hence, it can be suggested that micro-galvanic corrosion in the retained austenite has led to its selective dissolution as suggested in some literature (Della-Rovere et al 2013; Antony et al 2010; Potgieter et al. 2008).

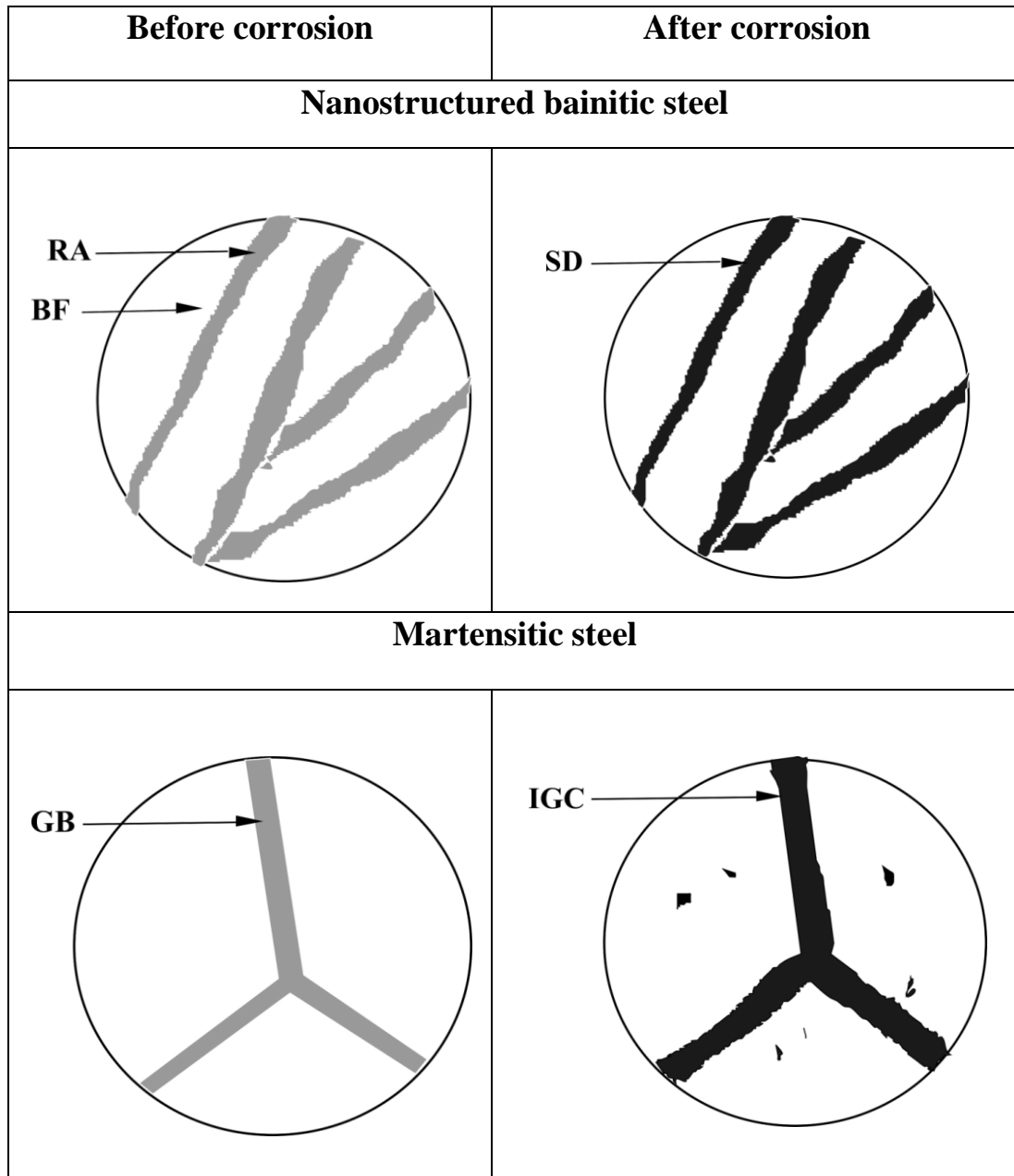


**Figure 4.7** A schematic representation of the microstructures of nanostructured bainitic steel and martensitic steel before and after corrosion in 3.5 wt. % NaCl solution (note *RA* is retained austenite, *BF* is bainitic ferrite, *SD* is selective dissolution, *GB* is grain-boundary and *IGC* is intergranular corrosion)

In the case of martensitic steel, a typical intergranular corrosion as well as localized corrosion in the matrix were observed, which could be due to carbon segregation along the grain boundaries and the matrix (Flis et al. 2009). Based on the electrochemical experiments and post-corrosion analysis, it is evident that the corrosion resistance of nanostructured bainitic steel is higher than martensitic steel. It well-known that localized corrosion in materials will affect the mechanical integrity under loading conditions, a phenomenon known as environment assisted cracking (Kannan et al. 2012). Hence, one could expect that the nanostructured bainitic steel would perform better than the martensitic steel in load-bearing structural applications when exposed to corrosive environments.

#### **4.2 Selective Dissolution of Retained Austenite**

To understand the corrosion mechanism of nanostructured bainitic steel, i.e., confirm the dissolution of the retained austenite, two nanostructured bainitic steels having different percentages of the retained austenite were studied.

##### ***4.2.1 Microstructure***

The representative TEM micrographs of the two nanostructured bainitic steels (200 °C and 350 °C steel) are shown in Figure 4.8. The bainitic ferrite laths and retained austenite films differ in volume and size for both steels. This is attributable to volume of the austenitic structure (obtained at 1100 °C) that finally gets transformed to ferritic structure at the low isothermal temperatures. Therefore the bainitic structure formed at isothermal temperature of 350 °C had bainitic ferrite laths and untransformed retained austenite films with an average thickness of  $300\pm 100$  nm and  $70\pm 30$  nm, respectively. The microstructure was significantly refined at the isothermal temperature of 200 °C. The steel contained nanosized

bainitic ferrite laths with an average thickness of  $60 \text{ nm} \pm 10 \text{ nm}$  and very fine retained austenite films (i.e.  $30 \pm 10 \text{ nm}$ ). The retained austenite volume fraction also decreased from  $53 \pm 1 \text{ wt.}\%$  at  $350 \text{ }^\circ\text{C}$  to  $21 \pm 2 \text{ wt.}\%$  at  $200 \text{ }^\circ\text{C}$  (Timokhina et al. 2011).

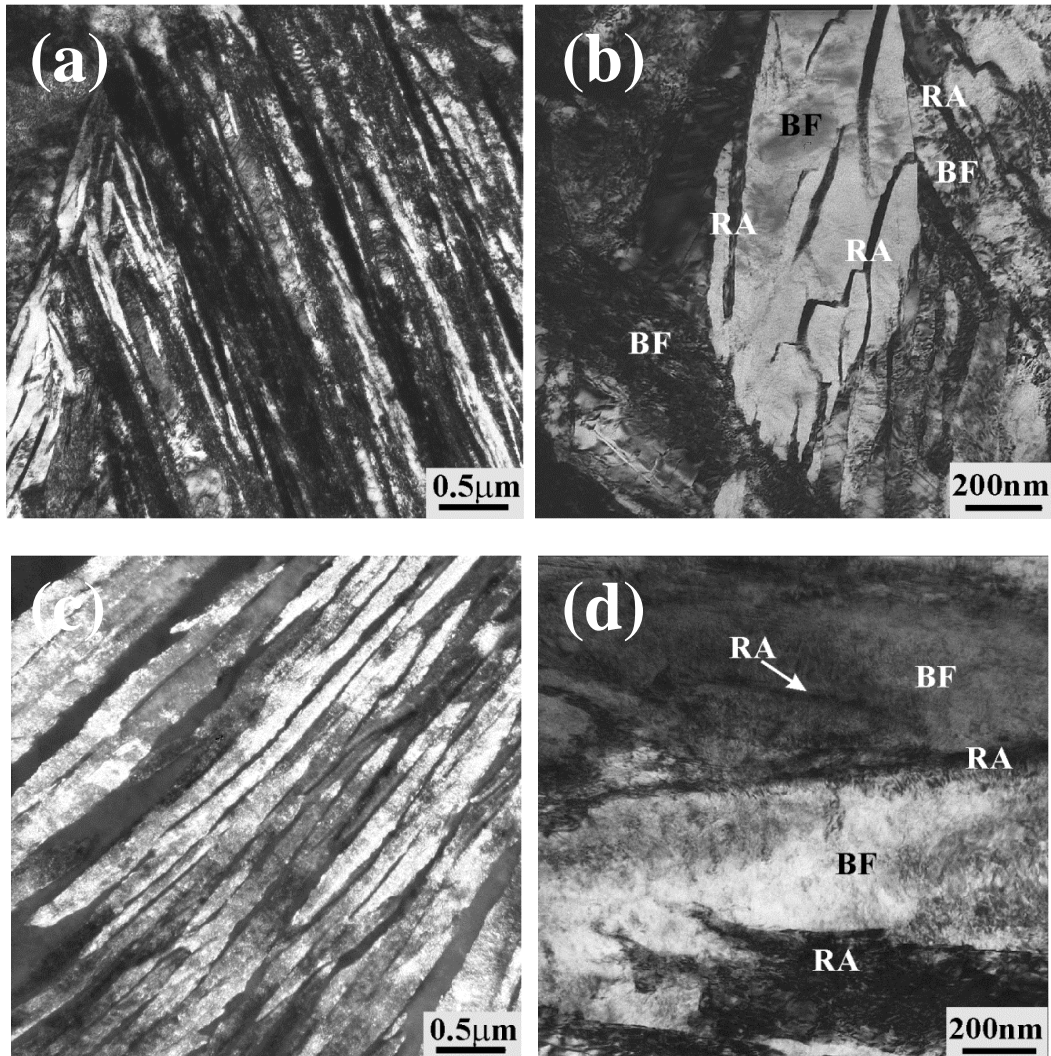


**Figure 4.8** TEM micrographs of the nanostructured bainitic steels formed at: (a and b)  $200 \text{ }^\circ\text{C}$  low and (c and d)  $350 \text{ }^\circ\text{C}$  (note: dark region are retained austenite, and bright regions are bainitic ferrite)

#### 4.2.2 Potentiodynamic Polarisation

The potentiodynamic polarisation curves of the nanostructured bainitic steels are shown in Figure 4.9. The corrosion current density ( $i_{corr}$ ) calculated from the

anodic curves showed a lower  $i_{corr}$  (higher corrosion resistance) for nanostructured bainitic steel formed at 200 °C steel than that at 350 °C. The  $i_{corr}$  for the nanostructured bainitic steels was  $0.776 \pm 0.4 \mu\text{A}/\text{cm}^2$  and  $3.98 \pm 0.5 \mu\text{A}/\text{cm}^2$  for 200 °C and 350 °C isothermal temperatures, respectively. The cathodic curves for both the steels showed diffusion controlled process, probably due to oxygen reduction reaction. However, the cathodic current density for the 200 °C steel was slightly lower than the 350 °C steel.

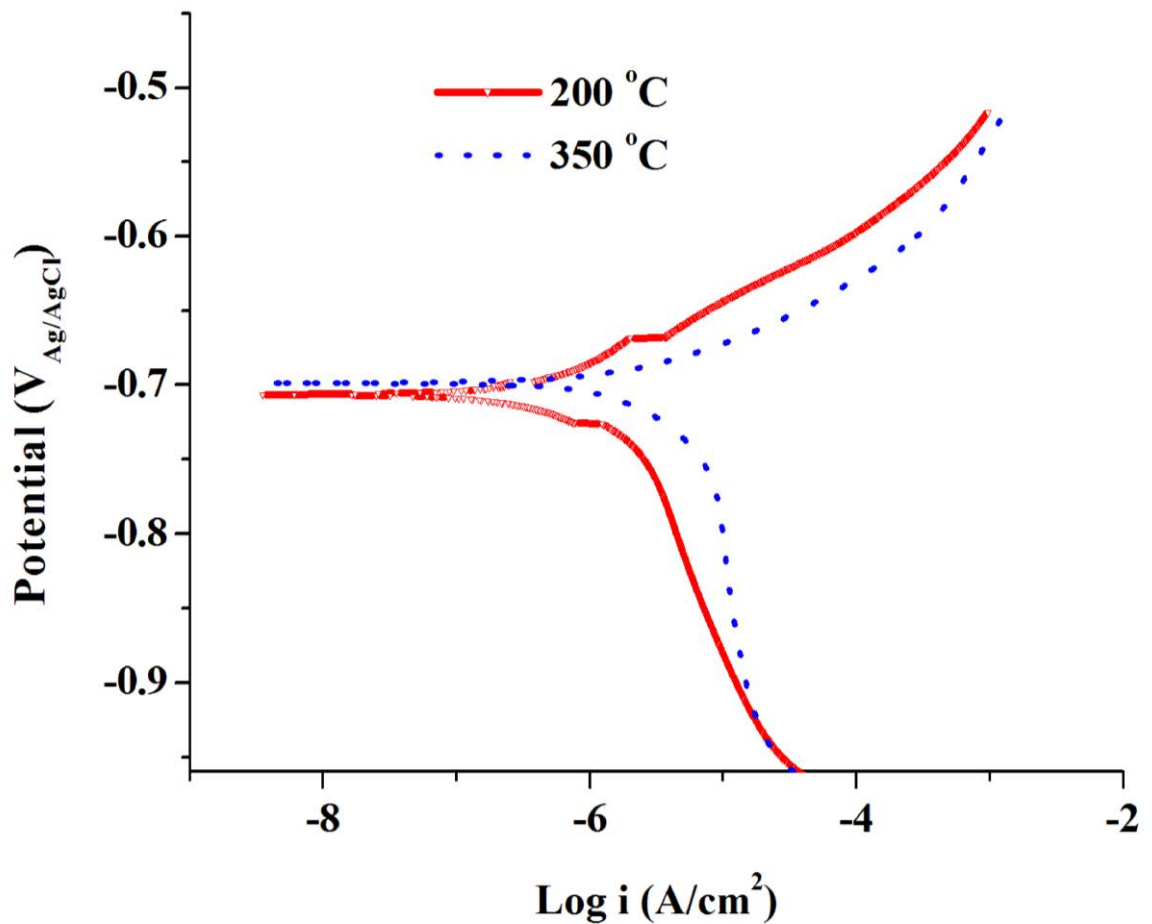


**Figure 4.9** Potentiodynamic polarisation curves for nanostructured bainitic steels

### 4.2.3 Post-Corrosion Analysis

Figure 4.10 shows the SEM micrographs of galvanostatically polarised samples. In the case of nanostructured bainitic steel formed at 200 °C, the corrosion attack appears to be more uniform (Figure 4.10(a)). However, a closer look at the surface revealed fine parallel streaks, probably as a result of selective dissolution of one phase (Figure 4.10(b)). The 350 °C bainitic microstructure, however, showed high corrosion attack and the morphology was also noticeably different to that of nanostructured bainite at 200 °C.

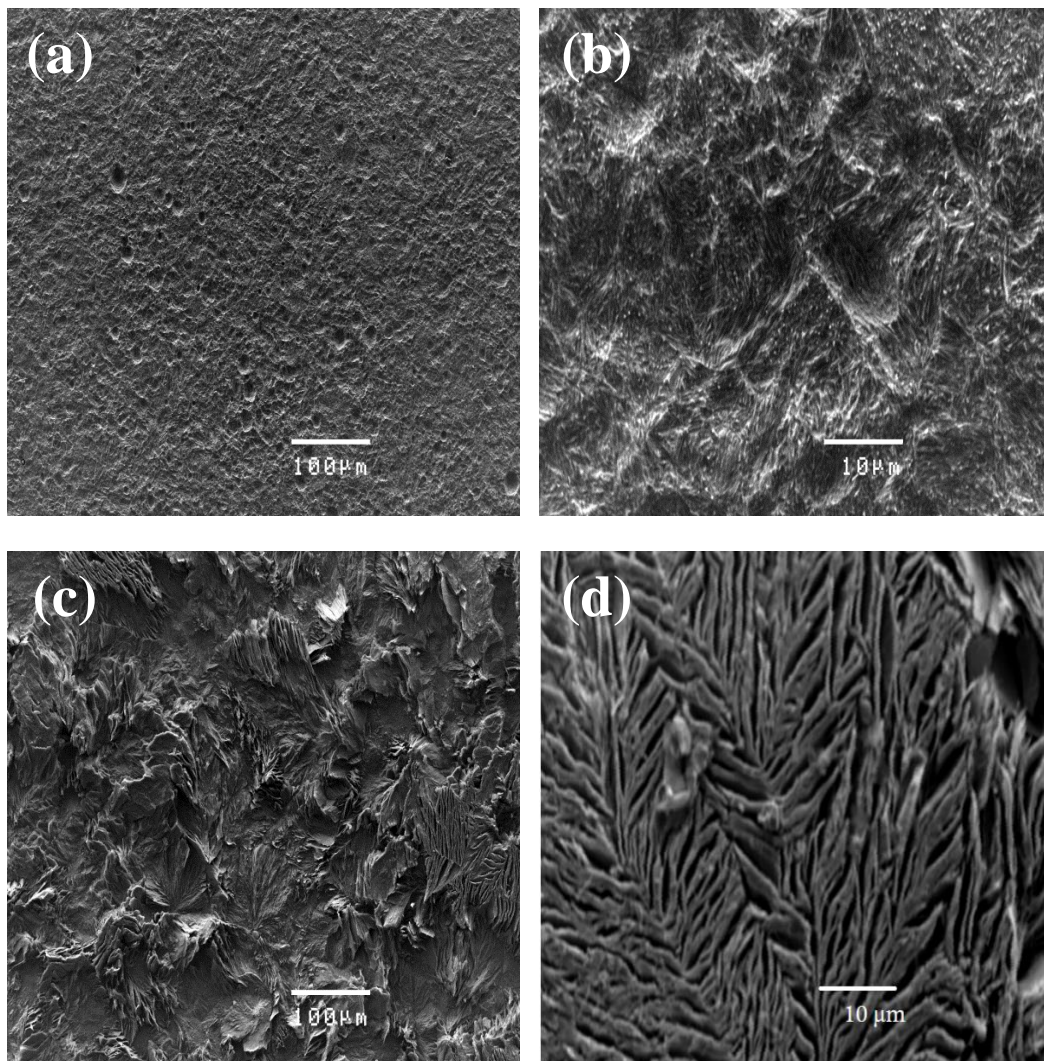


**Figure 4.10** SEM micrographs for galvanostatically polarised nanostructured bainitic steels formed at: (a and b) 200 °C and (c and d) 350 °C

Patches of fully and partly corroded regions can be seen in the 350 °C condition (Figure 4.10(c)). A higher magnification of the partially attacked region revealed a lamellar structure (Figure 4.10(d)), which clearly suggests selective dissolution of one phase. Comparing with the TEM micrographs (Figure 4.8), it can be suggested that the retained austenite has selectively dissolved in both the steels.

#### ***4.2.4 Discussion***

Literature suggests that the carbon content of the retained austenite films are significantly higher than in nanobainitic ferrite laths (Timokhina et al. 2011; Peet et al. 2004 Caballero et al. 2010; Tehovnik et al 2011). Furthermore the carbon distribution in the austenite exhibit a non-uniform pattern with distinct regions of both carbon enriched and carbon depleted zones (Zhang and Kelly 1998). It was reported that carbon particles (passive and cathodic in nature) (Mouri et al. 2002) can affect corrosion by forming confined regions at the particle/substrate interface where increasing concentration of reaction products favour anodic dissolution of surrounding carbon depleted zone of the austenite phase (Flis et al. 2009; Song et al. 1999). This could have influenced the more active austenite phase to undergo higher dissolution as compared to the bainitic ferrite. Interestingly, nanostructured bainitic steel of 200 °C, which also contained retained austenite, did not show such a prominent attack as that of 350 °C. This could be explained by noting that: (i) the volume fraction of retained austenite in the nanostructured bainite after 200 °C isothermal treatment is significantly lower (20 wt.%) than that of microstructure bainite (53 wt.%) after 350 °C treatment and (ii) the lath thickness of the retained austenite for 200 °C steel is finer than for 350 °C steel.

### **4.3 Summary**

Electrochemical experiments showed that the corrosion resistance of the nanostructured bainitic steel was higher as compared to that of the martensitic steel in chloride-containing solution. The martensitic steel revealed high localized corrosion, i.e., the grain boundaries were attacked predominantly leading to intergranular corrosion. However, the nanostructured bainitic steel revealed only a marginal selective dissolution of the retained austenite. Long-term immersion test confirm that the corrosion resistance of nanostructured bainitic steel was higher than that of the martensitic steel. The mechanism responsible for the different corrosion attack was discussed and found to be due to the difference in the microstructure of the steels. The nanostructured bainite formed at 200 °C was marginally more resistance to corrosion as compared with the bainitic structure transformed at 350 °C. Retained austenite undergoes selective dissolution and the localized corrosion attack was prominent when the lathe thickness was larger as in the case of nanostructured bainite formed at 350 °C.

## **CHAPTER 5: ELECTROCHEMICAL COATING OF POLYANILINE ON NANOSTRUCTURED BAINITIC STEEL**

The corrosion behavior of nanostructured bainitic steel suggests that a coating protection method is required for its widespread applications. Hence, in this study, the nanostructured bainitic steel was coated with a conducting polymer polyaniline (PANI) using galvanostatic method. The performance of the coatings was evaluated using electrochemical techniques in 3.5 wt. % NaCl solution.

### ***5.1 Galvanostatic Coating***

The potential–time (E-t) curves for the galvanostatic polymerisation of aniline using different coating current densities are shown in Figure 5.1. The potential of the sample increases with increasing the current density during the coating process. For the sample coated at low current density of  $5 \text{ mA cm}^{-2}$ , the potential gradually increased from 1.1 V until it stabilizes at around 1.8 V after about 900 s. When a high current density was used, higher potentials were recorded. In the case of  $20 \text{ mA cm}^{-2}$ , a sharp increase in the potential, i.e., 1.7 to 2.6 V was observed within 20 s, which then stabilized. The coating produced with low current density ( $5 \text{ mA cm}^{-2}$ ) showed a potential-time curve that was smooth, whereas the curves for high current density ( $10$  and  $20 \text{ mA cm}^{-2}$ ) were not smooth after 150 s. This can be attributed to the evolution of oxygen bubbles at high potentials. Coating was observed to form on the onset of the experiment as the substrate colour changed to black immediately.

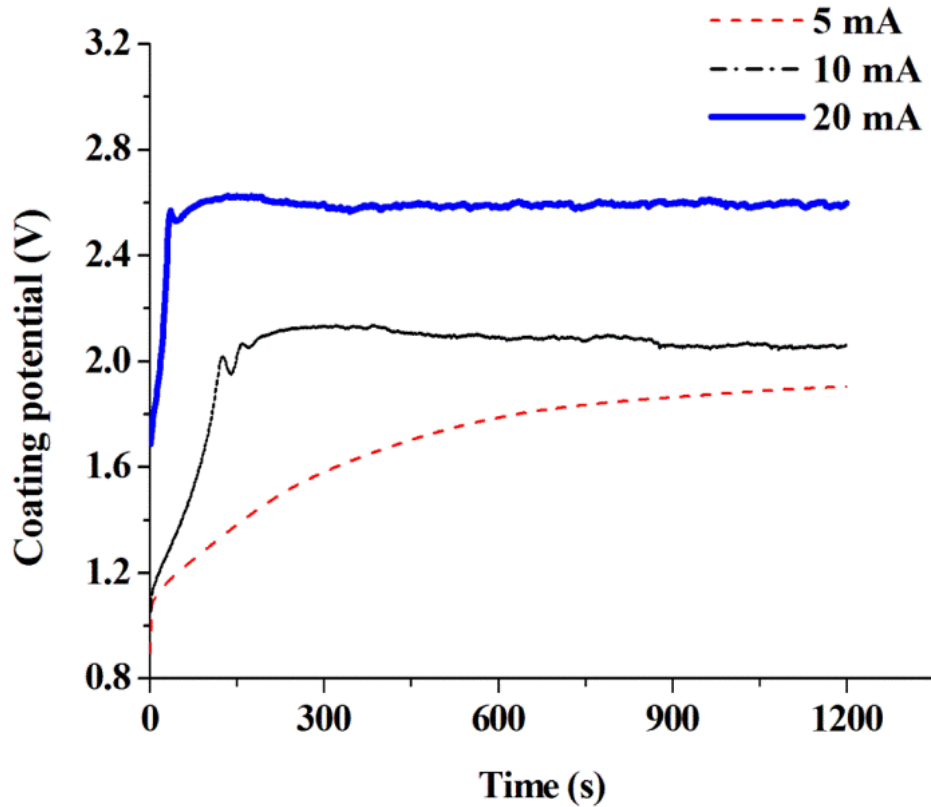


**Figure 5.1** Potential vs. time curves for galvanostatic synthesis of aniline coating on steel

### 5.2 Electrochemical impedance spectroscopy (EIS)

The Nyquist plots of the bare metal and the coated samples are shown in Figure 5.2. The plots were modelled using an equivalent circuit  $R(C(R(CR)))$  which consists of solution resistance ( $R_s$ ), polymer film resistance ( $R_f$ ), film capacitance ( $C_f$ ), charge transfer resistance ( $R_{ct}$ ) and double layer capacitance ( $C_{dl}$ ). The polarisation resistance,  $R_p$ , was calculated by adding  $R_f$  and  $R_{ct}$  (Pawar et al. 2006) Table 5.1 shows the coating thickness and respective  $R_p$  values for the samples. The higher  $R_p$  values from EIS results suggest that PANI coating using galvanostatic technique has significantly improved the corrosion resistance of the bare metal. The bare metal exhibited an  $R_p$  of  $3400 \Omega \text{ cm}^2$ , whereas the coated sample generally showed an  $R_p$  value from a range of  $\sim 5 \text{ k}\Omega \text{ cm}^2$  to  $32 \text{ k}\Omega \text{ cm}^2$ . The coating produced with  $1 \text{ mA cm}^{-2}$  has the lowest  $R_p$  value ( $5.3 \text{ k}\Omega \text{ cm}^2$ ) which

is due to the lower coating thickness. The coating with a current density of (5 mA cm<sup>-2</sup>) distinctively showed two capacitive loops and therefore a much better coating performance than the coating done at the higher current densities (10 mA cm<sup>-2</sup> and 20 mA cm<sup>-2</sup>) which revealed only a single loop.

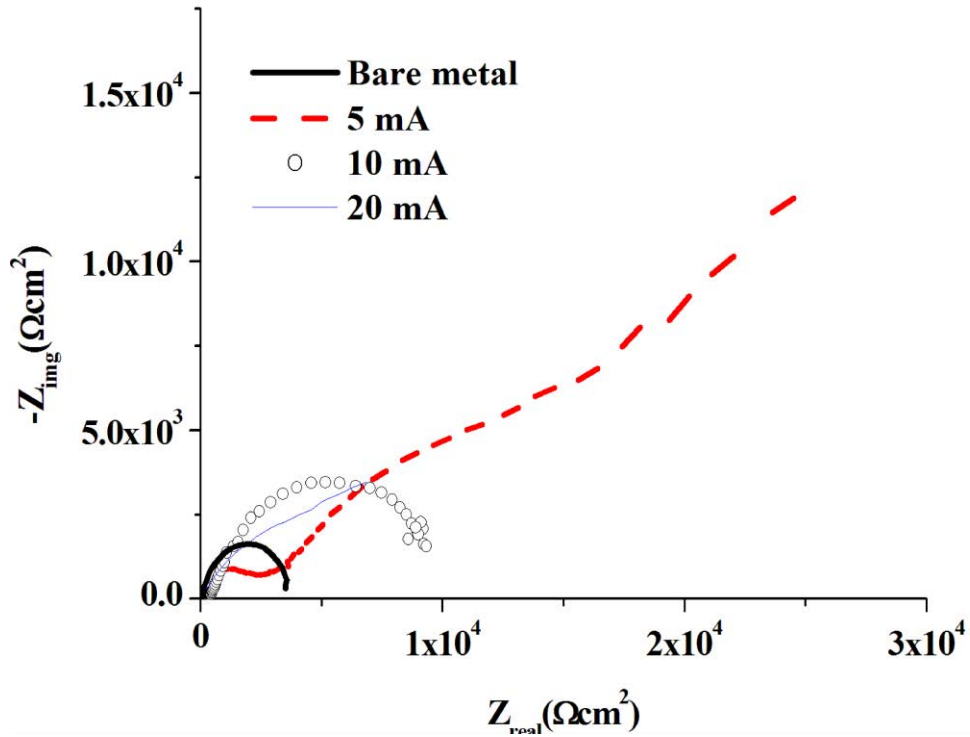


**Figure 5.2** Nyquist plot for bare metal and coated samples

**Table 5.1** EIS data of bare metal and coated samples

| Coated sample | $R_p$ (KΩ cm <sup>2</sup> ) | Average coating thickness (μm) |
|---------------|-----------------------------|--------------------------------|
| Bare metal    | 3.4 (± 0.03)                | -                              |
| 1 mA/10 min   | 5.3 (± 0.02)                | 6.12                           |
| 5 mA/10 min   | 32 (± 1.33)                 | 17.21                          |
| 10 mA/10 min  | 9.73 (± 0.14)               | 16.11                          |
| 20 mA/10 min  | 9.82 (± 0.20)               | 15.13                          |

### 5.3 Potentiodynamic Polarisation

The potentiodynamic polarisation curves for the bare and coated samples are shown in Figures 5.3. The corrosion potentials ( $E_{corr}$ ) of the coated samples were shifted toward the noble potential as compared to that of the bare metal. Table 5.2 is the potentiodynamic polarisation data for the bare metal and coated sample.

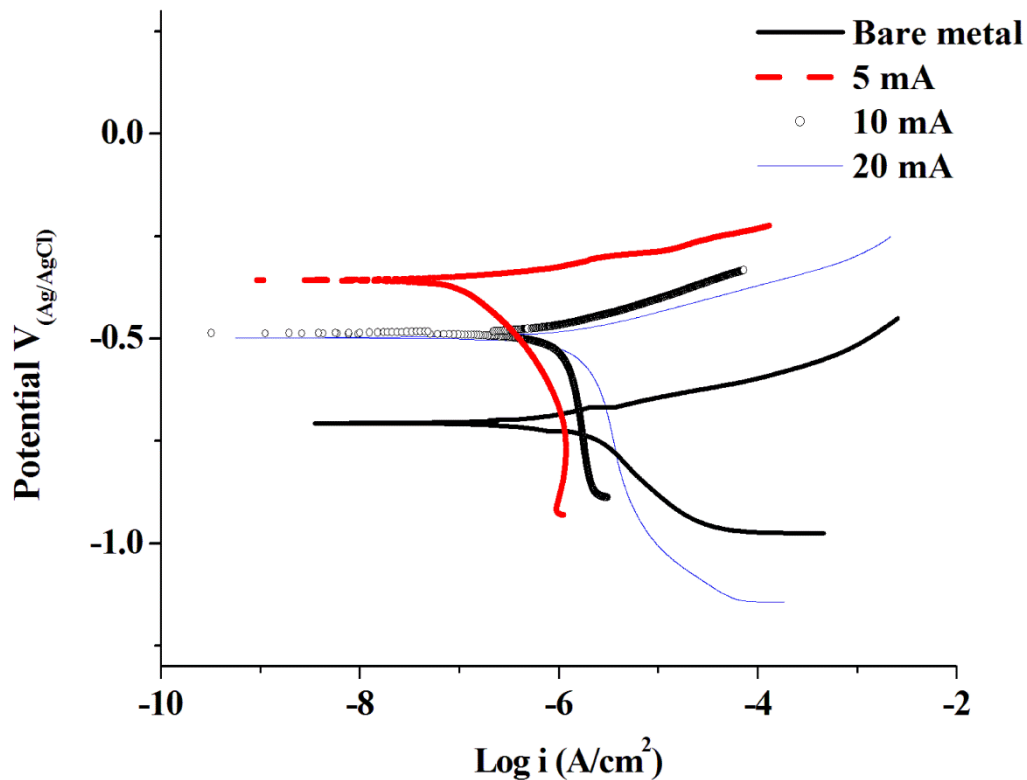


**Figure 5.3** Potentiodynamic polarisation plot for bare metal and coated samples

The bare metal showed an  $E_{corr}$  of -0.71 V and the values for the coated samples at various current densities are shown in Table 5.2. The  $E_{corr}$  exhibited by 5 mA cm<sup>-2</sup> and 20 mA cm<sup>-2</sup> current density for the coatings were -0.36 V and -0.50 V respectively. These values revealed a shift which is more to the positive potential. It was also noted that the coating produced with 1 mA cm<sup>-2</sup> current density has a poorer performance of the corrosion potential possibly due to the small coating thickness (~ 6 μm).

**Table 5.2** Potentiodynamic polarisation data for bare metal and coated samples

| Coated sample | $E_{corr}$ (V)   | $i_{corr}$ ( $\mu\text{A}/\text{cm}^2$ ) | Average coating thickness ( $\mu\text{m}$ ) |
|---------------|------------------|--|---|
| Bare metal    | $-0.71 \pm 0.01$ | $0.78 \pm 0.10$                          | -   |
| 1 mA/10 min   | $-0.63 \pm 0.00$ | $1.20 \pm 0.02$                          | 6.12  |
| 5 mA/10 min   | $-0.36 \pm 0.01$ | $0.15 \pm 0.12$                          | 17.21                                       |
| 10 mA/10 min  | $-0.49 \pm 0.00$ | $1.28 \pm 0.02$                          | 16.11                                       |
| 20 mA/10 min  | $-0.50 \pm 0.01$ | $2.23 \pm 0.01$                          | 15.13                                       |

However, the cathodic and anodic polarisation curves showed lower corrosion current for the coated samples compared to the bare metal which suggest corrosion resistance has been enhanced. Importantly, the corrosion current density ( $i_{corr}$ ) of the bare metal ( $0.78 \mu\text{A}/\text{cm}^2$ ) has dramatically reduced to ( $0.15 \pm 0.12 \mu\text{A}/\text{cm}^2$ ) for 5 mA  $\text{cm}^{-2}$  coated sample. The anodic curve for the 5 mA  $\text{cm}^{-2}$  coated sample also showed much lower corrosion current suggesting a better corrosion resistance when compared to that of 20 mA  $\text{cm}^{-2}$  ( $i_{corr} \sim 2.23 \mu\text{A}/\text{cm}^2$ ). This confirms the higher corrosion resistance performance of 5 mA  $\text{cm}^{-2}$  current density coated sample.

#### 5.4 Coating Characterization

In order to understand the performance of the coating, SEM analysis was done on the samples coated with 5 mA  $\text{cm}^{-2}$  and 20 mA  $\text{cm}^{-2}$  current density. The SEM micrographs of the coatings are shown in Figures 5.4. The coating produced with 5 mA  $\text{cm}^{-2}$  current density appeared compact with a few small pores ( $\sim 2.5 \mu\text{m}$ ) compared to that done with a high current density.

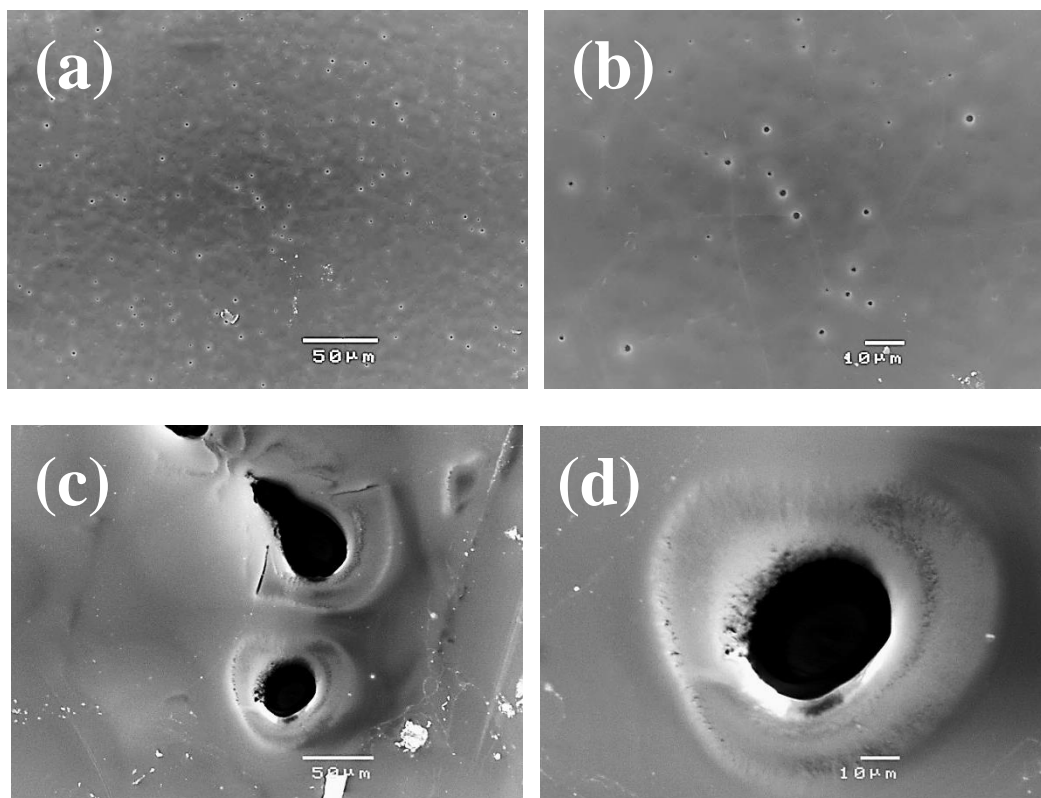


**Figure 5.4** SEM micrographs for galvanostatic coatings (a and b)  $5 \text{ mA cm}^{-2}$  (c and d)  $20 \text{ mA cm}^{-2}$

**Table 5.3** Coating thickness data for PANI coated steels

| Coated sample | Average coating thickness ( $\mu\text{m}$ ) |
|---------------|---|
| 1 mA/10 min   | 6.12  |
| 5 mA/10 min   | 17.21                                       |
| 10 mA/10 min  | 16.11                                       |
| 20 mA/10 min  | 15.13                                       |

Larger pores ( $\sim 50 \mu\text{m}$ ) can be observed on the sample that was produced using a  $20 \text{ mA cm}^{-2}$  current density. The pores generally can be attributed to oxygen

evolution on the sample, which visibly grew larger with higher current density. This oxygen evolution is thought to interfere with the formation of a uniform and compact coating resulting in coating with different porosity. The better performance of the coating produced with the current density of  $5 \text{ mA cm}^{-2}$  is attributable to the smaller pores and is demonstrated by its higher  $R_p$  value. The more compact the coatings the better the barrier between the sample and the stimulated sodium chloride environment (Martyak et al. 2002) as can be seen in the SEM micrographs Figures 5.4. Conversely, the coating produced with higher current density ( $20 \text{ mA cm}^{-2}$ ) exhibited larger pores and lower coating thickness of ( $\sim 15 \text{ }\mu\text{m}$ ) compare to that which was produced with current density of  $5 \text{ mA cm}^{-2}$  ( $\sim 17 \text{ }\mu\text{m}$ ) Table 5.3. This pore size and coating thickness can be attributed to the fact that the major portion of the current density in the  $20 \text{ mA cm}^{-2}$  coating was consumed in the oxygen evolution reaction and only a smaller portion was involved in the coating.

### ***5.5 Effect of Coating Time***

The effect of coating time (5, 10 and 20 min) was investigated for the coating done using a current density of  $5 \text{ mA cm}^{-2}$ . The Nyquist plots for the  $5 \text{ mA cm}^{-2}$  coated sample obtained at various coating time are shown in Figures 5.5 and 5.6. The  $R_p$  value increased with longer coating time. The  $R_p$  value was 20, 32 and  $110 \text{ K}\Omega \text{ cm}^2$  for 5, 10 and 20 min, respectively, with the highest  $R_p$  for the longest coating period (20 min). Long-term exposure tests showed that the  $R_p$  ( $110 \text{ K}\Omega \text{ cm}^2$ ) dropped to  $\sim 30 \text{ K}\Omega \text{ cm}^2$  in 72h. The potentiodynamic polarisation plot (Figure 5.7) showed a lower  $i_{corr}$  ( $0.09 \text{ }\mu\text{A/cm}^2$ ) for 20 min coating than for 10 min coating ( $0.15 \text{ }\mu\text{A/cm}^2$ ).

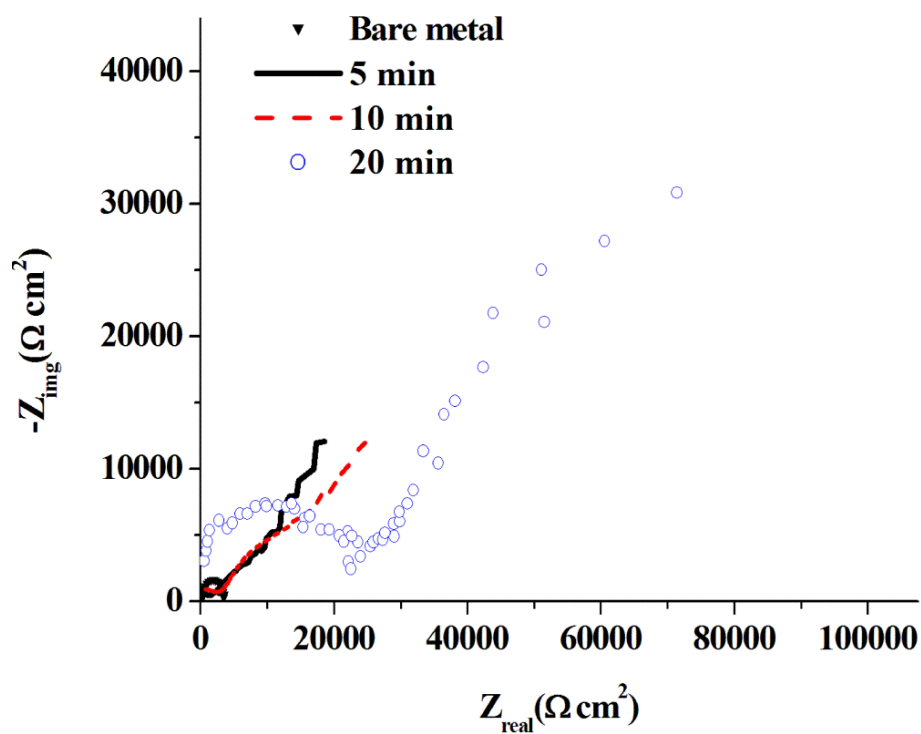


**Figure 5.5** Nyquist plot for the  $5 \text{ mA cm}^{-2}$  coated sample obtained at various coating time

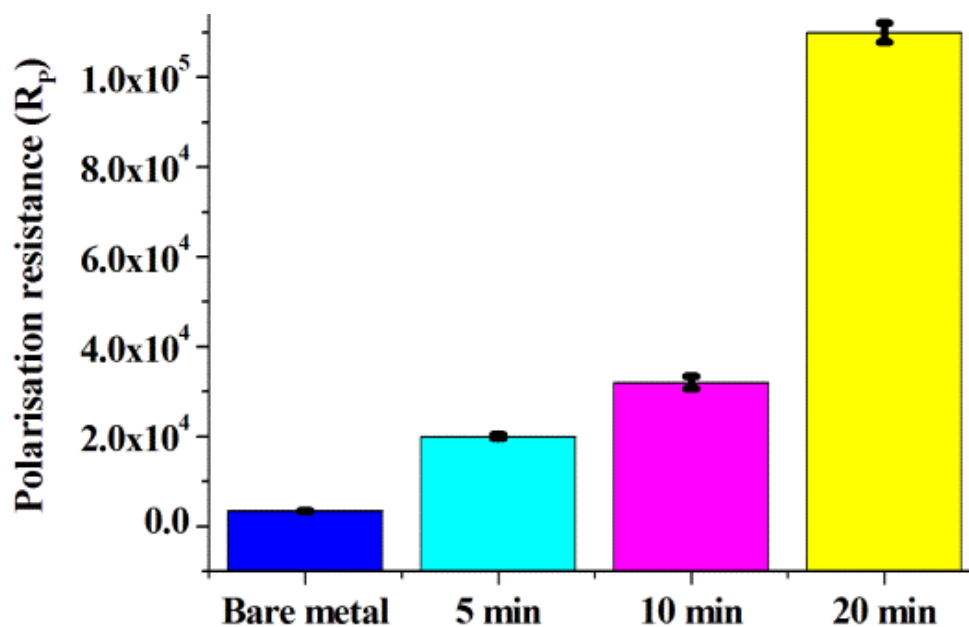


**Figure 5.6** Bar charts of  $R_p$  values for  $5 \text{ mA cm}^{-2}$  coated sample obtained at different coating time

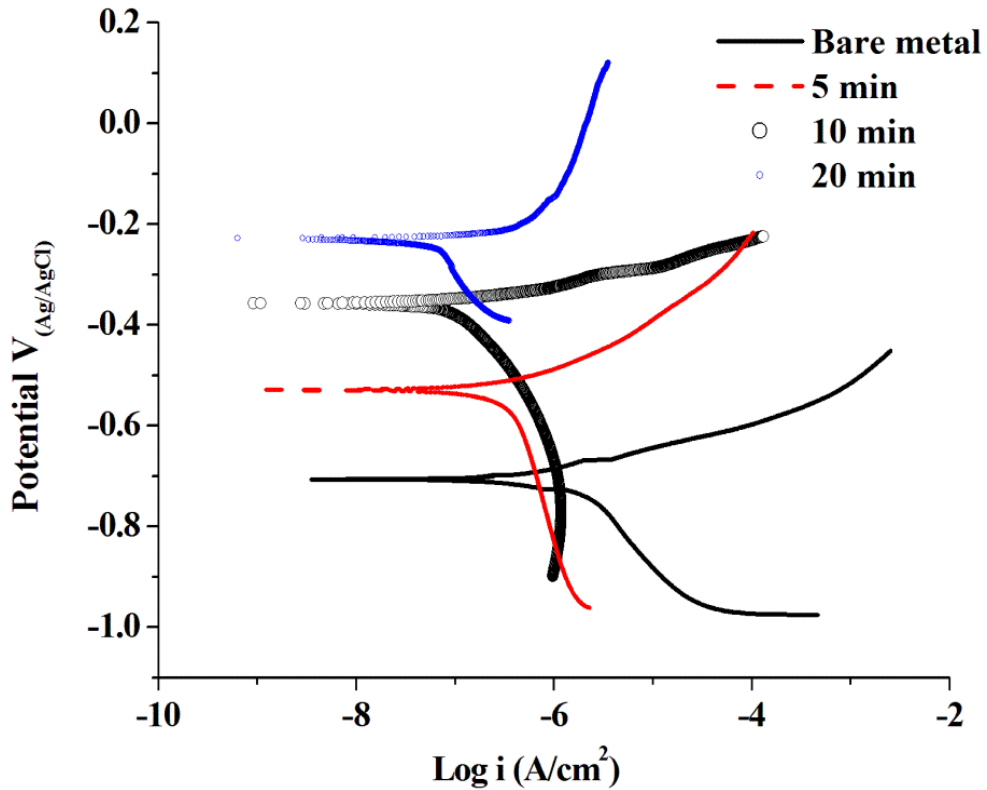


**Figure 5.7** Potentiodynamic polarisation plot for coated sample done with 5 mA cm<sup>-2</sup>

## 5.6 Effect of Stirring on Galvanostatic Coating

In order to reduce the porosity and thereby enhance the coating performance, a high current density of 20 mA cm<sup>-2</sup> was used to coat the steel under stirred-condition of the electrolyte.

### 5.6.1 Coating Potential

Figure 5.8 shows the transient potential vs. elapsed time plots for the galvanostatic polymerisation of aniline under two different bath conditions. In the case of unstirred condition, a sharp increase in potential (1.7-2.5 V) was observed in the first 30 s and then the potential became relatively stable. In the case of stirred condition, the potential gradually increased (1.58-2.4 V) with time.

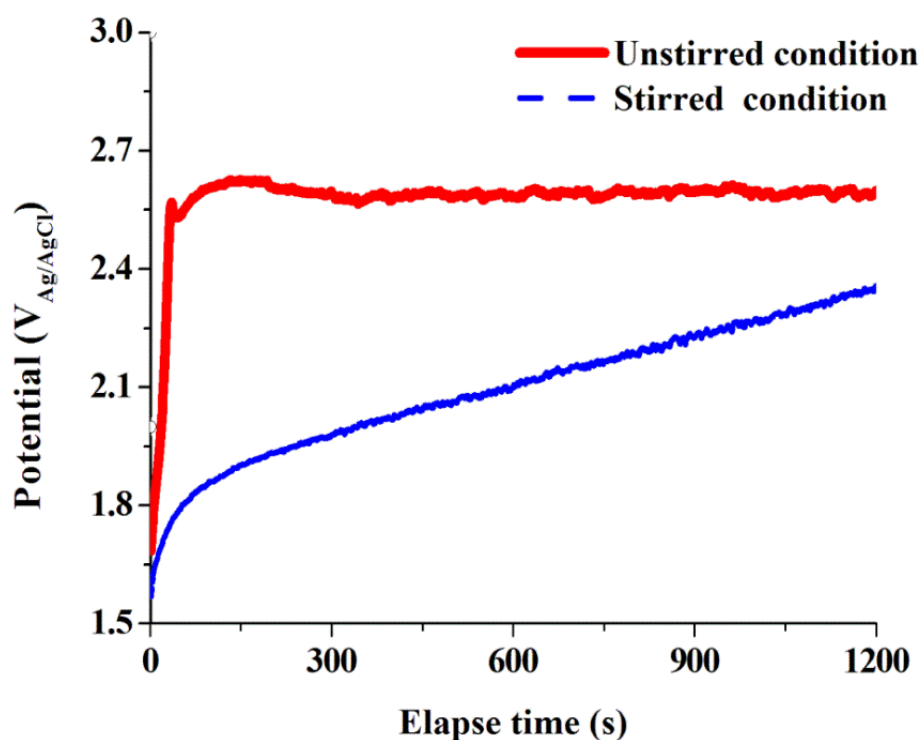


**Figure 5.8** Galvanostatic curves of polyaniline coatings on steel under two different electrolyte bath conditions

The polymerisation of aniline started immediately on the steel for both the conditions with a characteristic change of the colour of the substrate to black. However, a large number of bubbles were formed on the steel under unstirred-condition, whereas the bubble formation was drastically reduced under stirred-condition. Based on the potential of the steel during the coating process, it can be suggested that the bubbles are due to oxygen evolution reaction ( $2\text{H}_2\text{O} \rightarrow \text{O}_2 + 4\text{H}^+ + 4\text{e}^-$ ).

### 5.6.2 Coating Morphology

The SEM micrographs of the coatings (unstirred-condition coated (UC) and stirred-condition coated (SC)) are shown in Figure 5.9. A large number of defects can be observed in the UC sample, while only a few fine defects are observed in

the SC sample. The higher defects in the coating of the UC sample can be attributed to the formation of large bubbles on the sample, which interferes with the polymerisation of aniline. In fact, this phenomenon had an effect on the adhesion of the coating as well, i.e., high bubble formation on the UC sample reduced the adhesive strength of the coating. The SC and UC samples exhibited adhesive strength of  $3.5\pm 0.1$  N/mm<sup>2</sup> and  $3.1\pm 0.1$  N/mm<sup>2</sup>, respectively. Further, the average coating thickness of the SC sample (22  $\mu$ m) was higher than that of the UC sample (15  $\mu$ m), even under constant current coating. There are two possibilities for the increase in the coating thickness for SC sample: (i) reduction in oxygen evolution reaction, i.e., the stirring would have reduced the growth of oxygen bubbles by detaching them from the base metal and eventually producing a relatively uniform coating, and (ii) increase in the polymerisation due to effective mass transfer of the monomer (aniline) during the electrolyte stirring process.

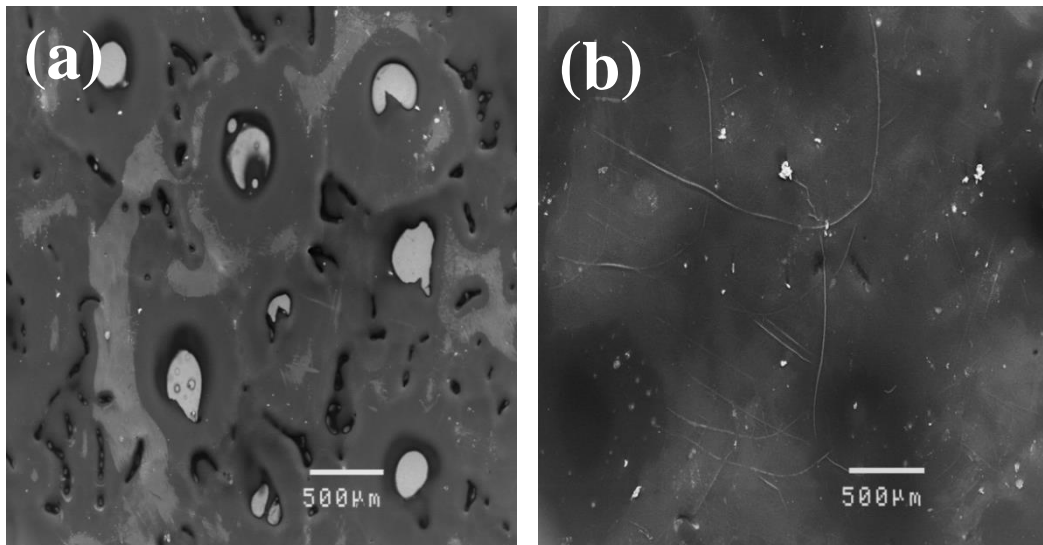


**Figure 5.9** SEM micrographs of polyaniline coatings on steel under two electrolyte bath conditions

### 5.6.3 Fourier Transform Infrared Spectroscopy (FTIR)

The FTIR spectra of the SC and UC samples are shown in Figure 5.10. The spectra for both the samples were similar, which indicates that there is no difference in the chemistry of the coating. The band observed at  $1593\text{ cm}^{-1}$  indicates quinoid (Q) ring stretching (Tang et al. 1988; Neoh et al. 1991) and the band at  $1483\text{ cm}^{-1}$  and  $1380\text{ cm}^{-1}$  correspond to stretching of the benzoid (B) rings (Tang et al. 1988; Ohsaka et al. 1984; Zheng et al. 1996) and C-N stretching in QB-Q surroundings (Neoh et al. 1991), respectively.

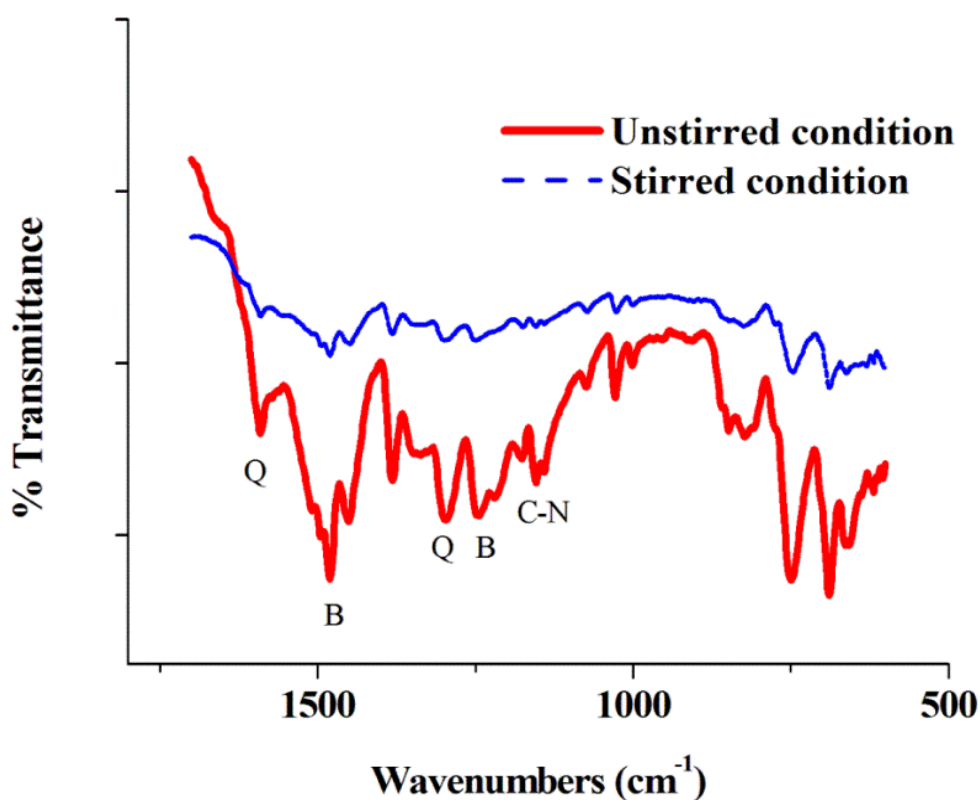


**Figure 5.10** FTIR spectra of polyaniline coating on steel produced using galvanostatic method under two different electrolyte bath conditions

The band at  $1252\text{ cm}^{-1}$  is representative of carboxylic group of the sodium salicylate in the coating (Camalet et al. 2000). The evidence of the Q and B bands

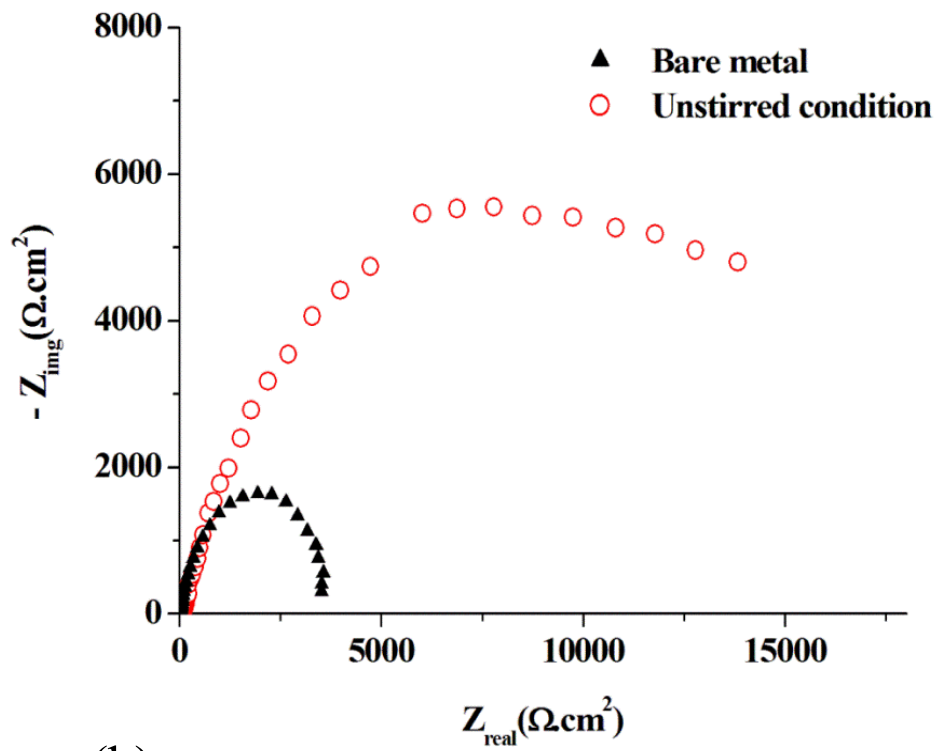
for both the coatings indicates polyaniline formation on the substrate. Further, the bands at  $1177\text{ cm}^{-1}$  and  $1023\text{ cm}^{-1}$  indicate 1-4 substitution on benzene rings, while for bands between  $800\text{ cm}^{-1}$  and  $700\text{ cm}^{-1}$  were indicative of 1-3 substitutions.

#### **5.6.4 Electrochemical Impedance Spectroscopy (EIS)**

The Nyquist plots of the bare metal and the coated samples are shown below in Figure 5.11. The EIS plots were modelled using an equivalent circuit which consists of solution resistance ( $R_s$ ), polymer film resistance ( $R_f$ ), film capacitance ( $C_f$ ), charge transfer resistance ( $R_{ct}$ ) and double layer capacitance ( $C_{dl}$ ). The EIS data obtained from the equivalent circuit modelling is given in Table 5.4. The polarisation resistance,  $R_p$ , was calculated by adding  $R_f$  and  $R_{ct}$  (Tuken et al. 2006). The EIS results suggest that PANI coating has significantly improved the corrosion resistance of the steel. The bare metal exhibited an  $R_p$  of  $3.4\text{ K}\Omega\text{ cm}^2$ , whereas the UC sample showed an  $R_p$  of  $16\text{ K}\Omega\text{ cm}^2$ . Importantly, the stirring of the electrolyte bath has further increased the performance of the coating. The SC sample exhibited an  $R_p$  of  $1500\text{ K}\Omega\text{ cm}^2$  which is almost two orders of magnitude higher than the UC sample. In order to understand the long-term performance of the coatings, EIS experiments were conducted over different exposure period in chloride-containing solution.

The  $R_p$  values obtained from the long-term EIS experiments for the coated samples are shown in Figure 5.12. For the UC sample, the  $R_p$  decreased drastically with increase in exposure time. There was a large drop in the  $R_p$  after 24 h exposure ( $R_p = 5.0\text{ K}\Omega\text{ cm}^2$ ) and then it gradually decreased over time to an  $R_p$  of  $1.2\text{ K}\Omega\text{ cm}^2$ .

(a)



(b)

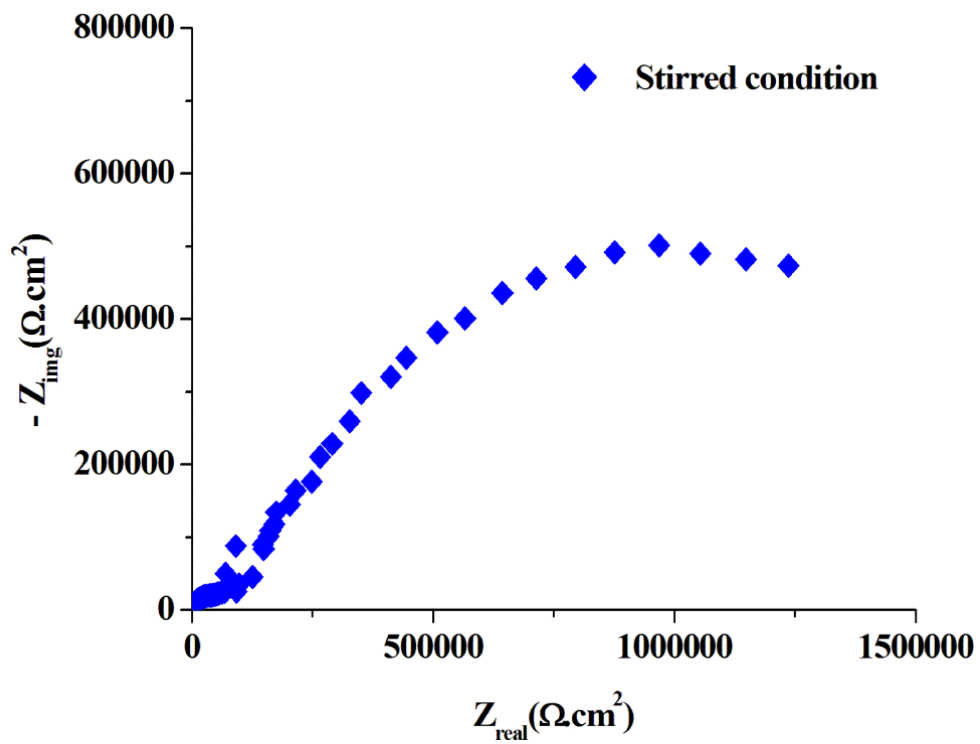


**Figure 5.11** Nyquist plots of bare metal and polyaniline coated samples tested in 3.5 wt. % NaCl solution

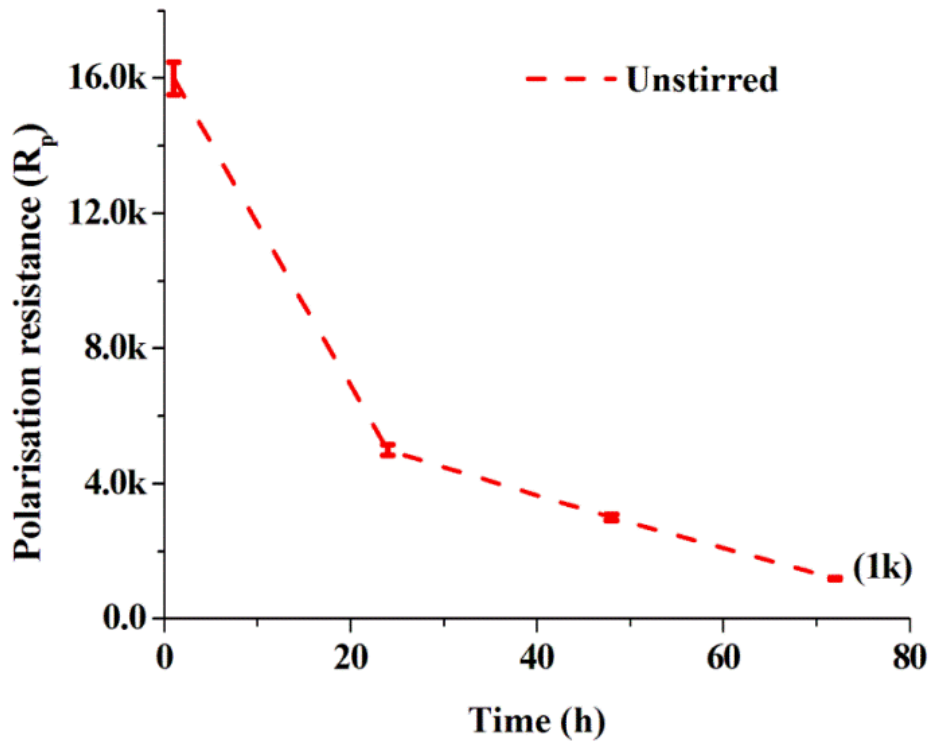
Interestingly, the SC sample showed an initial increase in the  $R_p$  value, which reached a peak  $R_p$  of  $4300 \text{ K}\Omega \text{ cm}^2$  after 72 h exposure. This can be attributed to the passivation mechanism provided by the redox chemistry of the conducting polymers (Camalet et al. 2000).

**Table 5.4** EIS values obtained from the fit to the equivalent circuit for the impedance spectra in 3.5 wt. % NaCl solution

|                                    | Bare metal                     | Unstirred condition             | Stirred condition                |
|------------------------------------|--------------------------------|---------------------------------|----------------------------------|
| $R_f(\Omega \cdot \text{cm}^2)$    | $2.60(0.1) \times 10^2$        | $6.09(\pm 0.10) \times 10^2$    | $8.15(\pm 0.20) \times 10^4$     |
| $C_f(\text{F}/\text{cm}^2)$        | $4.36(\pm 0.0) \times 10^{-5}$ | $7.26(\pm 0.30) \times 10^{-7}$ | $3.15(\pm 0.40) \times 10^{-10}$ |
| $R_{ct}(\Omega \cdot \text{cm}^2)$ | $3.10(\pm 0.03) \times 10^3$   | $1.57(\pm 0.04) \times 10^4$    | $13.41(\pm 0.10) \times 10^5$    |
| $C_{dl}(\text{F}/\text{cm}^2)$     | $6.34(\pm 0.0) \times 10^{-5}$ | $6.06(\pm 0.10) \times 10^{-7}$ | $9.98(\pm 0.03) \times 10^{-8}$  |
| $R_p(\Omega \cdot \text{cm}^2)$    | $3.40(\pm 0.03) \times 10^3$   | $1.60(\pm 0.10) \times 10^4$    | $15.00(\pm 0.20) \times 10^5$    |

However, the  $R_p$  of the SC sample started to decrease with increase in exposure period, i.e. the  $R_p$  decreased to  $\sim 700 \text{ K}\Omega \text{ cm}^2$  after 168 h exposure. It should be noted that the  $R_p$  of SC sample even after 168 h exposure was more than two orders of magnitude higher than that of the UC sample after 72 h exposure.

(a)



(b)

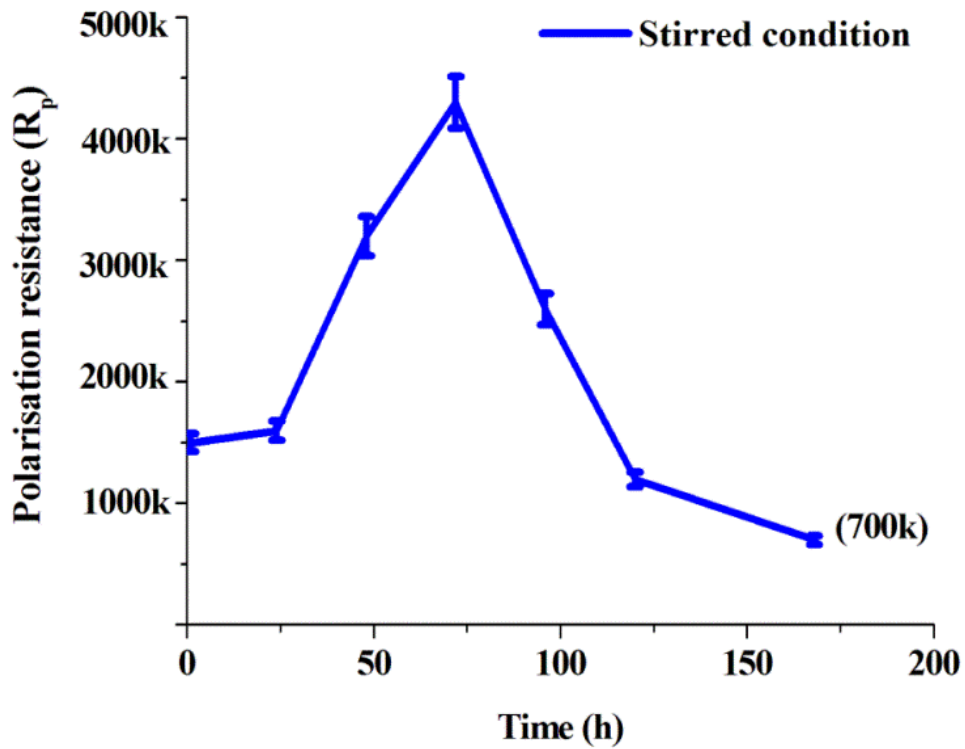


**Figure 5.12** Long-term polarisation plot of polyaniline coating on steel in 3.5 wt. % NaCl solution for electrolyte in (a) unstirred (b) stirred condition

### 5.6.5 Potentiodynamic Polarisation

The potentiodynamic polarisation curves for the bare and coated samples are shown in Figure 5.13. The corrosion potentials of the coated samples were shifted towards the noble direction as compared the bare metal. The bare metal showed an  $E_{corr}$  of -0.71 V and the UC and SC samples exhibited  $E_{corr}$  of -0.53 V and -0.01 V, respectively (Table 5.5). It was noted that the shift in the  $E_{corr}$  towards the noble direction for SC sample was significantly higher (~740 mV) than that of UC sample (~220 mV). This can be attributed to the less porosity of the SC coated sample which gives a better barrier protection.

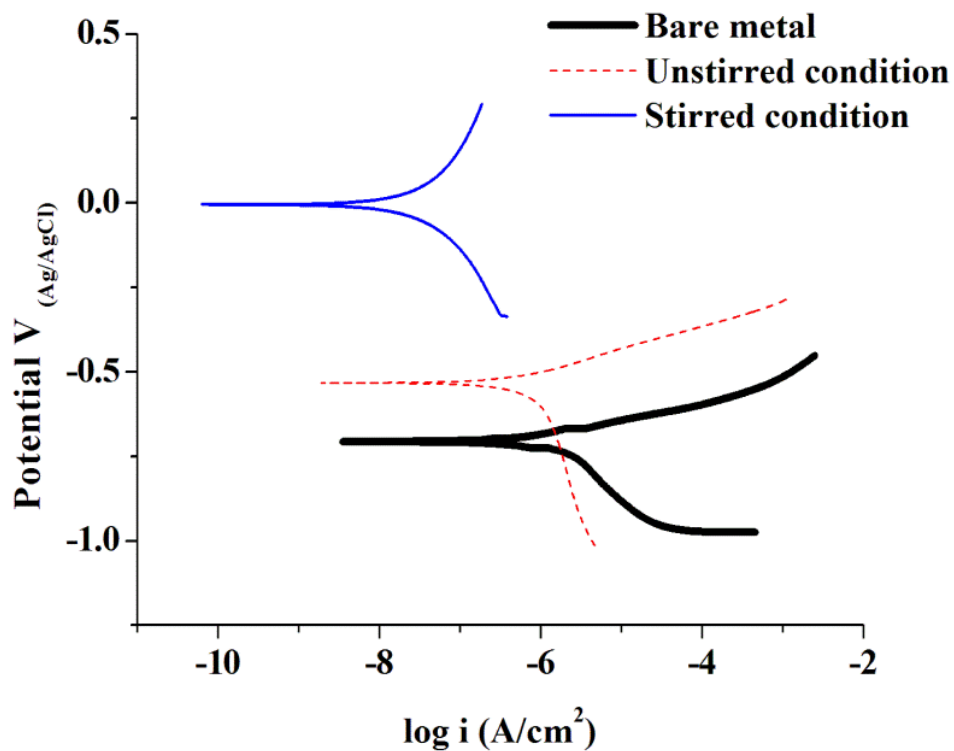


**Figure 5.13** Potentiodynamic polarization plots for the bare metal and the polyaniline coated samples tested in 3.5 wt. % NaCl solution

Importantly, the corrosion current density ( $i_{corr}$ ) of the steel ( $0.78 \mu\text{A}/\text{cm}^2$ ) has dramatically reduced in the case of SC sample ( $0.01 \mu\text{A}/\text{cm}^2$ ) as compared to that of UC sample ( $0.50 \mu\text{A}/\text{cm}^2$ ). This confirms the high performance of SC sample

and the positive effect of stirring the electrolyte bath during aniline polymerisation on the steel.

**Table 5.5** Electrochemical corrosion data for the bare sample and polyaniline coated samples tested in 3.5 wt. % NaCl solution

|   | Bare metal       | Unstirred condition | Stirred condition |
|---|------------------|---------------------|-------------------|
| $i_{\text{corr}}(\mu\text{A}/\text{cm}^2)$          | $0.78 \pm 0.04$  | $0.50 \pm 0.05$     | $0.01 \pm 0.00$   |
| $E_{\text{corr}}(\text{V}_{\text{Ag}/\text{AgCl}})$ | $-0.71 \pm 0.01$ | $-0.53 \pm 0.003$   | $-0.01 \pm 0.00$  |

### 5.7 Summary

Electrochemical synthesis of aniline coating on steel from aqueous sodium salicylate resulted in the formation of an adherent coating. This coating reliability was tested by electrochemical techniques.

Experimental results showed that the corrosion resistance tendency of PANI coated steel was significantly higher than that bare metal in 3.5 wt % NaCl solution. Electrochemical experiments clearly showed that polyaniline coating can be improved under galvanostatic technique by stirring. The coating produced on steel in an electrolyte bath with stirring performed better than the coating in the unstirred bath. The stirring of the coating solution inhibited oxygen bubbles growth and thereby reduced the defects in the coating. As a result, the steel coated in stirred condition revealed passivation and exhibited significantly high polarisation resistance even under long-term exposure.

## Chapter 6: Conclusions

### 6.1 General Conclusion

The corrosion performance of nanostructured bainitic steel was compared with martensitic steel in chloride-containing solution using electrochemical techniques. Electrochemical impedance spectroscopy (EIS) results showed that the polarisation resistance ( $R_p$ ) for nanostructured bainitic steel was higher than that of martensitic steel. Potentiodynamic polarisation results confirmed the higher corrosion resistance of nanostructured bainitic steel as compared to martensitic steel. Galvanostatic polarisation of the steels revealed steel intergranular corrosion (IGC) for martensitic and the selective dissolution of one phase of nanostructured bainitic steel.

Nanostructured bainite formed at 200 °C (retained austenite (RA): 21%) exhibited marginally higher corrosion resistance compared with that at 350 °C (retained austenite (RA): 53%). The localised corrosion attack was due to the selective dissolution of the retained austenite phase. The higher volume fraction and larger size of retained austenite in the 350 °C steel as compared to that of the 200 °C steel contributed to the higher corrosion attack in the 350 °C steel.

The corrosion resistance of the nanostructured bainitic steel was enhanced using polyaniline (PANI) coating. Galvanostatic coating method showed that lower current density and higher coating time increased the  $R_p$  of the coated samples. Under long-term exposure the  $R_p$  of the coated samples dropped drastically, which was attributed to the large pores in the coatings. However, the coating produced under stirred-condition of the electrolyte exhibited only a few fine defects and

hence showed significantly higher long-term corrosion resistance as compared to that of unstirred-condition coated samples.

## **6.2 Future Work**

It is generally known that high strength steels are prone to another form of localized corrosion known as stress corrosion cracking (SCC). Hence, it is important to study the synergetic effect of stress and corrosive environment on the nanostructured bainitic steel.

The coating process using galvanostatic method under stirred condition could be further improved by employing low current density under stirred condition to reduce oxygen evolution and also associated cost. However, the coating time should be optimized to produce a desirable coating thickness for better protection.

## REFERENCES

- Aeiyach, S., Zaid, B., Lacaze, P. C. (1999). "A one-step electrosynthesis of PPy films on zinc substrates by anodic polymerization of pyrrole in aqueous solution." *Electrochim. Acta*, 44, 2889-2898.
- Antony, P. J., Singh R. K., Raman, R., and Kumar, P. (2010). "Role of microstructure on corrosion of duplex stainless steel in the presence of bacterial activity." *Corros. Sci.* 52, 1404–1412.
- Avishan, B., Garcia-Mateo, C., Yazdani, S., and Caballero, F. G. (2013). "Retained austenite thermal stability in a nanostructured bainitic steel." *Mater. Charact.*, 81, 105-110.
- Beladi, H., Adachi, Y., Timokhina, I., and Hodgson, P. D. (2009). "Crystallographic analysis of 218 nanobainitic steels", *Scripta Mater*, 60, 455–458.
- Bhadeshia, H. K. D. H. (2005). "Large chunks of very strong steel." *Mater. Sci. Technol*, 21, 293–302.
- Bordbar, S., Alizadeh, M., and Hojjat-Hashemi, S. (2013). " Effects of microstructure alteration on corrosion behaviour of welded joint in API X70 pipeline steel." *Mater. Des.* 45, 597–604.
- Caballero, F. G., Miller, M. K., Clarke, A. J., and Garcia-Mateo, C. (2010). "Examination of carbon partitioning into austenite during tempering of bainite." *Scripta. Mater.*, 63, 442-445.
- Caballero, F. G., and Bhadeshia, H. K. D. H. (2004). "Very strong bainite." *Curr. Opin. Solid State Mater. Sci.*, 8, 251–257.
- Caballero, F. G., Miller, M. K., Babu, S. S., and Garcia-Mateo, C. (2007). "Atomic scale observations of bainite transformation in a high carbon high silicon steel." *Acta. Mater.* 55, 381-390.
- Camlet, J. L., Lacroix, J. C., Aeiyach, S., Chane-Ching, K., and Lacaze, P. C. (1996). "Electrodeposition of protective polyaniline films on mild steel." *J. Electroanal. Chem.*, 416, 179-182.
- Camalet, J. L., Lacroix, J. C., Dung Nguyen, T., Aeiyach, S., Pham, M. C., Petit Jean, J., and Lacaze, P.C. (2000). "Aniline electropolymerization on platinum and mild steel from neutral aqueous media." *J. Electroanal. Chem.*, 485, 13-20.

Cascalheira, A. C., Aeiyaich, S., Lacaze, P. C., and Abrantes, L. M. (2003). "Electrochemical synthesis and redox behavior of polypyrrole coatings on copper in salicylate aqueous solution." *Electrochim. Acta.*, 48, 2523-2529.

Charlie, R. B. (1996). "Principles of heat treatment of plain carbon and alloy steels." USA: 2<sup>nd</sup> Print. ASM International- Technology and Engineering.

Chaudhari, S., Mandale. A. B., Patil, K. R., Sainkar, S. R., Patil, P. P. (2006). "Formation of poly (*o*-anisidine) coatings on copper from aqueous salicylate solution." *Surf. Coat. Tech.*, 200, 5557-5565.

Chen, X. H., Lu, J., Lu, L., and Lu, K. (2005). "Tensile properties of a nanocrystalline 316L austenitic stainless steel." *Scripta. Mater.* 52, 1039-1044.

CSIRO. (2008). "Corrosion cost" Viewed October, 2013." <<http://www.corrosion-club.com/costs.htm>>

Da-wei, J., Chang-sheng, G. E., Xiang-juan, Z., Jun, L., Lu-lu, S., and Xue-shan, X. (2012). "22Cr high Mn-N low-Ni economical duplex stainless steels." *J. Iron & Steel Res., Inter.*, 19(2), 50-56.

Della, C. A., Santos, F. S., Silva, R., Souza, C. A. C., and Kuri, S. E. (2013). "Influence of long term low-temperature aging on the microhardness and corrosion properties of duplex stainless steel." *Corros. Sci.* 68, 84–90.

Ehinger, D., Kruger, L., Martin, U., Weigelt, C., and Aneziris, C. G. (2013). "Temperature effects on the deformation behaviour of high-density trip steel and particle-reinforced trip steel/zirconia honeycombs under quasi-static compressive loading." *Adv. Eng. Mater.* 15, 646-657.

El-Shazly, A. H. and Al-Turaif, H. A. (2012). "Improving the corrosion resistance of buried steel by using polyaniline coating." *Int. J. Electrochem. Sci.*, 7, 211-221.

Finish Road Administration. (1995). "The final results of the road traffic in winter project." Viewed October 2013 <http://alk.tiehallinto.fi/winter.htm>

Flis, J., Ziomek-Moroz, M., and Flis-Kabulska, I. (2009). "Effect of carbon on corrosion and passivation of iron in hot concentrated NaOH solution in relation to caustic stress corrosion cracking", *Corros. Sci.* vol. 51 pp. 1696–1701.

Fontana, M. G. (1987). "Corrosion engineering." 3<sup>rd</sup> ed. Singapore: McGraw-Hill Book Company.

Furuhara, T., Kawata, H., Morito, S., and Maki, T. (2006). "Crystallography of upper bainite in Fe-Ni C alloys." *Mater. Sci. Eng. A*, 431, 228-236.

Garcia-Mateo, C., Caballero, F. G., and Bhadeshia, H. K. D. H. (2003). "Hard bainite." *ISIJ Int.* 43, 1238-1243.

Gamry Instrument. (2013). "Basics of electrochemical impedance spectroscopy." Viewed October 2013 <http://www.gamry.com.info@gamry.com>

Guo, J., Yang, S., Shang, C., Wang, Y., and He, X. (2008). "Influence of carbon content and microstructure on corrosion behaviour of low alloy steels in a Cl<sup>-</sup> containing environment." *Corros. Sci.*, 51, 242-251.

Gvozdenovic, M. M., Jugovic, B. Z., Stevanovic, J., Grgur, B. N., Trisovic, T. T., and Jugovic, Z. (2011). "Electrochemical synthesis and corrosion behavior of polyaniline-benzoate coating on copper." *Synthetic Met.*, 161, 1313-1318.

Herrasti, P., and Ocon, P. (2001). "Polypyrrole layers for steel protection." *Appl. Surf. Sci.*, 172, 276-284.

Kannan, M., and Dietzel, W. (2012). "Pitting-induced hydrogen embrittlement of magnesium–aluminium alloy." *Mater. Des.* 42, 321–326.

Kazum, O., Kannan, M., Beladi, H., Timokhina, I. B., Hodgson, P. D., and Khoddam, S. (2013). "Aqueous corrosion performance of nanostructured bainitic steel." *Material & Design*, 54, 67-71.

Kazum, O., Kannan, M., Beladi, H., Timokhina, I. B., Hodgson, P. D., and Khoddam, S. (2013). "Selective dissolution of retained austenite in nano-bainitic steel." *Advanced Engineering Material*,s 15, 1-3.

Kazum, O., and Kannan, M. 2013. "Galvanostatic polymerization of aniline on steel: improving the coating performance in chloride-containing environment." nano-bainitic steel." *Synthetic Metals* 180, 54-58..

Li, L., Celis, J. (2004). "Intergranular corrosion of 304 stainless steel pickled in acidic electrolytes." *Scripta Mater.*, 51, 949-953.

Martins, S., Decker, S., Kruger, L., Martins, U., and Rafaja, D. (2013). "Microstructure changes in trip steel/Mg-PSZ composites induced by low compressive deformation." *Adv. Eng. Mater*, 15, 600-608.

Martins, J. I., Reis, T. C., Bazzaoui, M., Bazzaoui, E .A., and Martins, L. I. (2004). "Polypyrrole coatings as a treatment for zinc-coated steel surfaces against corrosion." *Corros. Sci.* 46, 2361-2381.

Martins, J. I., Bazzaoui, M., Reis, T. C., Bazzaoui, E .A., and Martins, L. (2002). "Electrosynthesis of homogeneous and adherent polypyrrole coatings on iron and steel electrodes using a new electrochemical procedure." *Synthetic Met.*, 129, 221-228.

Martyak, N. M., Mcandrew, P., McCaskie, J .E., and Dijon, J. (2002). "Electrochemical polymerization of aniline from oxalic acid medium." *Prog. Org. Coat.*, 45, 23-32.

- Mouri, L., Mabile, I., Fiaud, C., and Amouroux, J. (2002). "Improvement of the corrosion resistance of a low carbon steel using a two step plasma treatment." *Corros. Sci.*, 44, 2089-2099.
- Neoh, K. G., Kang, E. T., and Tan, K. T. (1991). "Structural study of polyaniline films in reprotation/depotation cycles." *J. Phys. Chem.*, 95, 10151-10156.
- Kinlen, P. J., Sliverman, D. C., and Jeffreys, C. R. (1997). "Corrosion protection using polyaniline coating formulations." *Synthetic Met*, 85, 1327-1332.
- Kraljic, M., Mandic, Z., and Duic, L. J. (2003). "Inhibition of steel corrosion by polyaniline coatings." *Corros. Sci.*, 45, 181-198.
- Ogurtsov, N. A., Pud, A. A., Kamarchik, P., and Shapoval, G. S. (2004). "Corrosion inhibition of aluminum alloy in chloride mediums by undoped and doped forms of polyaniline." *Synthetic Met.*, 143, 43- 47.
- Ohsaka, T., Ohnuki, Y., Oyama, N., Katagiri, G., and Kamisako, K. (1984). "Ir absorption spectroscopic identification of electroactive and electroinactive polyniline films prepared by the electrochemical polymerization of aniline." *J. Electroanal. Chem.*, 161, 399-406.
- Parakala, S. R. (2005). "Galvanic corrosion aspect of stainless steel and black steel reinforcement in concrete." M.Sc. thesis, University of Ohio, Athens, Ohio, USA.
- Patil, S., Sainkar, S. R., Patil, P. P. (2004). "Poly (*o*-anisidine) coatings on copper: synthesis, characterization and evaluation of corrosion protection performance." *Appl. Surf. Sci.*, 225, 204-216.
- Pawar, P., Gaikawad A. B., and Patil, P. P. (2006). "Electrochemical synthesis of corrosion protective coating on mild steel from aqueous salicylate medium." *Sci. Technol. Adv. Mat.* 7, 723-744.
- Peet, M., Babu, S. S., Miller, M. K., and Bhadeshia, H. K. D. H. (2004). "Three-dimensional atom probe analysis of carbon distribution in low-temperature bainite." *Scripta. Mater.* 50, 1277-1281.
- Pereloma, E. V., Timokhina, I. B., Miller, M. K., and Hodgson, P. D. (2007). "Three-dimensional atomic probe analysis of solute distribution in thermomechanically processed trip steels." *Acta. Mater.*, 55, 2587-2598.
- Perren, R. A., Suter, T. A., Uggowitz, P. J., Weber, L., Magdowski, R., Bohni, H., and Speidel, M. O. (2001). "Corrosion resistance of super duplex stainless steels in chloride ion containing environments: investigations by means of a new microelectrochemical method I. precipitation-free states." *Corros. Sci.*, 43, 707-726.

- Petitjean, J., Aeiyaeh, S., Lacroix, J. C., and Lacaze, P. C. (1999). "Ultra-fast electropolymerization of pyrrole in aqueous media on oxidizable metals in a one-step process." *J. Electroanal. Chem.*, 478, 92-100.
- Potgieter, J. H., Olubambi, P. A., Cornish, L., Machio, C. N., and Sherif, E. M. (2008). "Influence of nickel additions on the corrosion behaviour of low nitrogen 22% Cr series duplex stainless steels." *Corros. Sci.*, 50, 2572–2579.
- Roberge, P. R. (2008). "Corrosion engineering, principles and practice." 1st ed. New York: Mc Graw Hill.
- Saidman, S. B., and Bessone, J. B. (2002). "Electrochemical preparation and characterization of polypyrrole on aluminum in aqueous solution." *J. Electroanal. Chem.*, 521, 87-94.
- Sajjadi, S. A., and Zebarjad, S. M. (2007). "Isothermal transformation of austenite to bainite in high carbon steels." *Journal on Materials Processing Technology*, 189, 107-113.
- Sarkar, P. P., Kumar, P., Manna, M. K., and Chakraborti, P. C. (2005). "Microstructural influence on the electrochemical corrosion behavior of dual-phase steels in 3.5% NaCl solution." *Mater. Lett.* 59, 2488-2491.
- Shinde, V., Sainkar, S. R., and Patil, P. P. (2005). "Corrosion protective poly (*o*-toluidine) coatings on Copper." *Corros. Sci.*, 47, 1352- 1369.
- Sitraam, S. P., Stoffer, J. O., Okeefe, T. J. (1997). "Application of conducting polymers in corrosion protection." *Mater. Research Center*, 69, 65-69.
- Song, G., and Atrens, A. (1999). "Corrosion mechanisms of magnesium alloys." *Adv. Eng. Mater.*, 1, 11-33.
- Srikanth, A. P., Sunitha, T. G., Raman, V., Nanjundan, S., Rajendran, N. (2007). "Synthesis, characterization and corrosion protection properties of poly(N-(acryloxymethyl) benzotriazole-co-glycidyl methacrylate coating on mild steel." *Materials Chemistry and Physics*, 103, 241-247.
- Subathira. A., and Meyyappan. R. (2010). "Electrodeposition and anti-corrosive properties of polypyrrole coatings on stainless steel." *Recent Research Sci. Tech.* 2(1), 124-129.
- Tang, J., Jing, X., Wang, B., and Wang, F. (1988). "Infrared spectra of soluble polyaniline." *Synth. Met.*, 24, 231–238.
- Tehovnik, F., Arzensek, B., Arh, B., Skobir, D., Pirnar, B., and Zuzek, B. (2011). "Microstructure evolution in SAF 2507 super duplex stainless steel." *Mater. Technol.* 45, 339–345.

Terada, M., Saiki, M., Costa, I., and Padilha, A. F. (2006). "Microstructure and intergranular corrosion of the austenite stainless steel 1.4970." *J. Nucl. Mater.*, 358, 40-46.

Timokhina, I. B., Beladi, H., Xiong, X. Y., Adachi, Y., and Hodgson, P. D. (2011). "Nanoscale microstructural characterization of a nanobainitic steel." *Acta Mater*, 59, 5511–5522.

Tuan, Y. H., Wang, C. S., Tsai, C. Y., Chao, C. G., and Liu, T. F. (2009). "Corrosion behaviors of austenitic Fe-30Mn-7Al-xCr-1C alloys in 3.5% NaCl solution." *Mater. Chem. Phys.*, 114, 595-598.

Tuken, T., Yazici, B., and Erbil, M. (2006). "The corrosion behavior of polypyrrole coating synthesized in phenylphosphonic acid solution." *Appl. Surf. Sci.*, 252, 2311-2318.

Wang, J., Li, G., Xiao, A. (2011) "A bainite-ferrite multi-phase steel strengthened by Ti-microalloying." *Mater. Trans.* 52, 2027-2031.

Wessling, B. (1994) "Passivation of metals by coating with polyaniline, Corrosion potential shift and morphological changes." *Adv. Mater.* 6, 226-228.

Wessling, B. (1997). "Scientific and commercial breakthrough for organic metals." *Synthetic Met.*, 85, 1313-1318.

Xue, X., Shan, Y., Zheng, L., and Lou, S. (2006). "Microstructural characteristic of low carbon microalloyed steels produced by thermo-mechanical controlled process." *Mater. Sci. Eng. A.*, 438-440, 285-287.

Yang, L. (2008). "Techniques for corrosion monitoring." 1<sup>st</sup> ed. England: Woodhead Publishing in Materials.

Yang, Z., and Fang, H. (2005). "An overview on bainite formation in steels." *Current Opinion in Solid state & Materials Sci.*, 9, 277-286.

Yao, B., Wang, G., Ye, J., and Li, X. (2008). "Corrosion inhibition of carbon steel by polyaniline Nanofibers." *Mater. Lett.*, 62, 1775-1778.

Yi, Y. S., Shoji, T. (1996). "Quantitative evaluation of material degradation of thermally aged duplex stainless steels using chemical immersion test." *J. of Nucl. Mater.*, 240, 62-69.

Zhang, M. X., and Kelly, P. M. (1998). "Determination of carbon content in bainitic ferrite and carbon distribution in austenite by using CBKLDP." *Mater. Charact.*, 40, 159-168.

Zhao, Y. T., Yang, S. W., Shang, C. J., Wang, X. M., Liu, W., He, X. L. (2007). "The mechanical properties and corrosion behaviors of ultra-low carbon microalloying steel." *Mater. Sci. Eng. A*, 454-455, 695-700.

Zheng, W. Y., Levon, K., Taka, T., Laakso, J., and Osterholm, J. E. (1996). "Doping-induced layered structure in N-alkylated polyaniline." *Polym. J.*, 28, 412–418.

Zhou, H. H., Jiao, S. Q., Chen, J. H., Wei, W. Z., Kuang, Y. F. (2004). "Relationship between preparation conditions, morphology and electrochemical properties of polyaniline prepared by pulse galvanostatic method (PGM)." *Thin Solid Films*, 450, 233-239.